New experimental density data and derived thermophysical properties of carbon dioxide – Sulphur dioxide binary mixture (CO2 - SO2) in gas, liquid and supercritical phases from 273 K to 353 K and at pressures up to 42 MPa

Accepted Manuscript

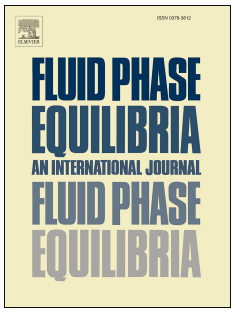

New experimental density data and derived thermophysical properties of carbon dioxide – Sulphur dioxide binary mixture (CO_2 - SO_2) in gas, liquid and supercritical phases from 273 K to 353 K and at pressures up to 42 MPa

Mahmoud Nazeri, Antonin Chapoy, Alain Valtz, Christophe Coquelet, Bahman Tohidi

PII: S0378-3812(17)30352-7

DOI: 10.1016/j.fluid.2017.09.014

Reference: FLUID 11586

To appear in: *Fluid Phase Equilibria*

Received Date: 6 July 2017

Revised Date: 15 September 2017

Accepted Date: 17 September 2017

Please cite this article as: M. Nazeri, A. Chapoy, A. Valtz, C. Coquelet, B. Tohidi, New experimental density data and derived thermophysical properties of carbon dioxide – Sulphur dioxide binary mixture (CO_2 - SO_2) in gas, liquid and supercritical phases from 273 K to 353 K and at pressures up to 42 MPa, *Fluid Phase Equilibria* (2017), doi: 10.1016/j.fluid.2017.09.014.

New experimental density data and derived thermophysical properties of carbon dioxide – Sulphur dioxide binary mixture (CO_2 - SO_2) in gas, liquid and supercritical phases from 273 K to 353 K and at pressures up to 42 MPa

Mahmoud Nazeri[a*], Antonin Chapoy[a,b*], Alain Valtz[b], Christophe Coquelet[b], Bahman Tohidi[a]

[a] *Hydrates, Flow Assurance & Phase Equilibria Research Group, Institute of Petroleum Engineering, Heriot-Watt University, Edinburgh, EH14 4AS, UK*

[b] *MINES ParisTech PSL Research University, CTP-Centre of Thermodynamics of Processes, 35, Rue Saint Honoré, 77305 Fontainebleau, France*

** Corresponding Authors:* *Mahmoud Nazeri (M.Nazeri@hw.ac.uk)*

Antonin Chapoy (A.Chapoy@hw.ac.uk)

ABSTRACT

Due in part to the toxicity of the CO_2-SO_2 binary system, there are no density data available in the literature. Densities for this system were measured using a vibrating tube densitometer (VTD), Anton Paar DMA 512, and the forced path mechanical calibration (FPMC) method in the gas, liquid and supercritical phases at pressures up to 41.7 MPa. The mole fraction of the mixture was 0.9478 CO_2 + 0.0522 SO_2 at 298 K and 0.9503 CO_2 + 0.0497 SO_2 at 273, 283, 323 and 353 K. The compressibility factor, isobaric heat capacity and bubble points were also derived from the measured densities. The classical cubic equations of state, i.e., Soave-Redlich-Kwong (SRK), Peng-Robinson (PR) and Valderrama version of Patel-Teja (VPT) with the CO_2 volume correction term and Peneloux shift parameter in addition to a multi parameter EoS based on Helmholtz energy were evaluated using the measured density data. The most accurate EoSs for the investigated system were the multi parameter EoS and the PR-CO_2 with overall AAD of 0.6% and 1.0%, respectively.

Keywords: *Density, Carbon capture transport and storage (CCS), CO_2, Sulphur Dioxide (SO_2), Thermophysical properties, Equation of State (EoS)*

1. Introduction

High demand for energy due to the rapid economic growth resulted in an ever increasing use of fossil fuels, i.e. coal, oil and natural gas following the industrial revolution. The effect of this has been to increase the amount of greenhouse gases such as CO_2 in the atmosphere. Carbon capture and storage (CCS) is the name given to technology based solutions aimed at reducing CO_2 emissions to the atmosphere [1]. This technology comprises capturing CO_2 during burning of fossil fuels, compression and transport mainly via pipelines and injection into geological storage basins. The captured CO_2 will contain ranges of impurities depend on the source of fossil fuel as well as the capturing technology [2][3].

Sulphur dioxide can be present in heavy oil production or in flue gas in the post-combustion or oxyfuel processes in coal-fired power plants. In the MEA-based absorption processes, impurities such as O_2, NO_2 and SO_2 can lead to severe operational problems such as foaming, viscosity increase and formation of heat-stable salts. The typical range of SO_2 in the MEA-based post-combustion processes is 500-3000 part per million by volume (ppm_v). Flue gas desulphurisation (FGD) units with wet SO_2 scrubbers can absorb 80-95% of the SO_2 in the flue gas before entering the CO_2 absorber. However, in case of failure in the FGD unit, 75% of the SO_2 could be absorbed by MEA as it is not selective a solvent to acid gases [2]. The presence of SO_2 can make problems such as corrosion in the presence of water [4] in the transportation of captured CO_2 with impurities from both MEA-based post-combustion or oxyfuel processes [5][6].

Due to the toxicity of SO_2, the Immediately Dangerous to Life and Health (IDLH) concentration of this component is set to 100 ppm_v by the National Institute for Occupational Safety and Health (NIOSH) [7]. Shell Cansolv also commissioned an integrated system to capture CO_2 and SO_2 simultaneously in a commercial scale post-combustion coal fired power plant in Saskatchewan. The captured CO_2 is transported for the CO_2 Enhanced Oil Recovery (CO_2-EOR) in Weyburn oil field and SO_2 is used to produce sulphuric acid as a valuable by-product [8].

Similar to injection of acid gases, i.e., injection of CO_2 - H_2S [9][10], technically, CO_2 and SO_2 can be co-stored in deep saline aquifers and this effectively reduces the capture cost by avoiding SO_2 removal costs [11][12][13]. However, the reactivity of SO_2 with rock in the presence of water and acids that form is an issue of concern [14][15][16]. The geochemical

effects can reduce the pH of the formation water, change the porosity of reservoir rock and cause mineral dissolution and sulphate precipitation [11][17][18][19][20].

A proper understanding of the thermodynamic and transport properties of CO_2-SO_2 systems is required as an input to feasibility studies and equipment sizing in the above processes [21]. The presence of impurities in the captured streams of CO_2 would affect the thermophysical properties, in particular density and viscosity, of high CO_2 content mixtures. Equations of state (EoSs) should be evaluated using the experimental density and vapour-liquid equilibrium (VLE) data. The lack of experimental data for CO_2-SO_2 systems is certainly due to toxicity of the system [22]. The only available data for this system is reported by Caubet [23] in 1904. A comprehensive thermodynamic behaviour of CO_2-SO_2 mixture was studied experimentally by Coquelet and co-workers [24], [25] for transport purposes of CO_2 mixtures in a CCS context. Only VLE data are available at 263.15 K and 333.21 K and at pressures ranging from 0.1 to 8.8 MPa.

In this work, the densities of approximately 95 mol% CO_2 with 5 mol% SO_2 were measured using a Vibrating Tube Densitometer (VTD) in the gas, liquid and supercritical phases. The measurements were carried out at five isotherms 273, 283, 298, 323 and 353 K at pressures up to 42 MPa. Thermodynamic properties such as compressibility factor, isobaric specific heat capacity and bubble points were obtained from the measured densities. The measured densities also were employed to evaluate the classical cubic EoSs, i.e., Soave-Redlich-Kwong (SRK-EoS) [26], Peng-Robinson (PR-ES) [27], and Valderrama modification of the [28] Patel-Teja (VPT-EoS) [29] EoSs. Then, to improve the density prediction, the CO_2 volume correction term [30] and Peneloux shift parameter [31] were introduced to those EoSs. Also, a multi parameter EoS based on Helmholtz energy [32][33] with the short industrial equation from Lemmon & Span for pure SO_2 [34] (see Appendix A) and Span &Wagner EoS for pure CO_2 [35] was evaluated using the measured density data and derived thermodynamic properties.

2. Experimental part

Experimental work was carried out in the high safety laboratory at CTP - Centre of Thermodynamics of Processes research group at Mines ParisTech in France.

2.1. Material

A binary mixture of CO_2-SO_2 was prepared to perform density measurements. Table 1 shows the details of the chemicals, suppliers and purities of the components used in this study. A pressure vessel with a volume of 100 mL was vacuumed and then after disconnecting from the vacuum pump, the mass was measured using a balance with four digit after the decimal point (brand: Sartorius) three times. Due to the lower vapour pressure of SO_2 (0.35 MPa at 293 K) compared to CO_2 (with a vapour pressure of 5.73 MPa at 293 K), first SO_2 was injected to the vacuumed pressure vessel. After neutralising the SO_2 trapped in the line using sodium hydroxide (NaOH) considering acid base reaction, the pressure vessel was disconnected and the weight was measured to obtain the exact amount of injected SO_2. The weight of injected SO_2 was 6.357 g. The pressure vessel then was connected to the CO_2 cylinder in order to inject CO_2. After disconnecting the pressure vessel and weighing with the balance, the amount of injected CO_2 was 79.229 g. After calculations, the mole percent for SO_2 and CO_2 was 5.22 mol% with $u_r(z)$ = 0.010 mol% 94.78 mol% with $u_r(z)$ = 0.180 mol%, respectively. The uncertainties are reported with 95% confidence level (coverage factor *k=2).* The prepared binary mixture was then used to perform density measurements at 298 K. Due to a leak through the piston to the nitrogen side resulting in a change in the composition, another binary mixture was prepared with a similar procedure to conduct the density measurements at the other isotherms. The amount of injected SO_2 and CO_2 was 4.579 and 60.183 g, respectively. The mole percent and uncertainties with 95% confidence level were 4.97 mol% with $u_r(z)$ = 0.010 mol% for SO_2 and 95.03 mol% with $u_r(z)$ = 0.181 mol% for CO_2, respectively.

2.2. Equipment description

A Vibrating Tube Densitometer (VTD), Anton Paar DMA 512 was used to measure the densities. Figure 1 shows a schematic view of the setup which has been thoroughly described in previous publication [36][37]. Briefly, the main part of the setup is a U-shaped vibrating tube Anton Paar densitometer (1) with a working pressure of up to 70 MPa and temperature range of 263 – 423 K. The tube material is Hastelloy. A jacket through which fluid is circulated from a liquid bath (4) surrounds the densitometer allowing control of the temperature with a stability of ±0.02 K. The sample fluid flows from the 150 ml, 70 MPa rated pressurised vessel (2) to the densitometer through a tube with a diameter of 1.6 mm

(1/16 inches) and pressure rating of 100 MPa. The connecting tubes are fully immersed in a temperature controlled liquid bath model West P6100 (5).

The pressure of setup is measured with three pressure transducers (model: Druck PTX611) (6) with ranges of 0-10 MPa, 10-30 MPa and 30-70 MPa. The transducers were calibrated with an electronic balance (model: GE Sensing PACE 5000) at pressure up to 20 MPa and using a dead weight tester (model: Desgranges & Huot 5202S) for pressures from 20 to 40 MPa. The pressure transducers can measure the pressure with standard uncertainties of $u(p)$ = 0.002 MPa , $u(p)$ = 0.005 MPa and $u(p)$ = 0.005 MPa in the ranges of 0-10 MPa, 10-30 MPa and 30-70 MPa, respectively. The temperature of the densitometer and the liquid bath were measured using four-wire 100-Ω platinum resistance probes (Pt100) (7). The probes were calibrated against a reference thermometer with 25-Ω (model: Tinsley Precision Instrument). The standard uncertainty of the temperature probes were estimated to be $u(T)$ = 0.02 K after calibration. The pressure and temperature were recorded using an Agilent HP34970A data acquisition unit (10). The vibration period, τ, also was recorded using a HP53131A data acquisition unit (10).

2.3. Calibration and measurement procedures

The densitometer was firstly calibrated using pure CO_2 as a reference fluid and forced path mechanical calibration (FPMC) model developed by Bouchot and Richon [38][39][40]. This method considers that the vibrating tube is represented by a box with a known internal volume, V, and a known mass of tube M_0. The box is connected to a support with a spring with a constant of stiffness, K. Consequently, the period of vibration, τ, is expressed by: $\tau = 2\pi\sqrt{\frac{M}{K}}$, with $M = M_0 + \rho V$. In this model, the stress and strain behaviour of the tube material would be represented from the realistic mechanical considerations. The reference fluid is used to set the magnitude of pressure independent from temperature. The following equation shows the frame for the FPMC model:

$$\rho = \left(\frac{M_0}{V_i(T,P)}\right)\left[\left(\frac{K(T,P)}{K_0(T)}\right)\left(\frac{\tau^2(T,P)}{\tau_0^2(T)}\right) - 1\right] \quad (1)$$

Where ρ is the density of inner fluid, M_0 is the mass of the tube under vacuum, V_i is the internal volume, K is the natural transversal stiffness and τ is the vibrating period. The subscript 0 indicates the vacuum condition. By considering the tube as a thick-walled cylinder and replacing terms for the M_0/V_i and K/K_0, the complete FPMC model can be formulated as [38]:

$$\rho(T,P) = \left(\frac{M_0}{L_{00}}\right)\left(\frac{1}{\pi r_i^2(T,P)\delta L(T,P)}\right)\left[\left(\frac{\Delta r^4(T,P)}{\Delta r_0^4(T)}\right)\exp(-3\gamma_T P)\left(\frac{\tau^2(T,P)}{\tau_0^2(T)}\right) - 1\right] \quad (2)$$

The density data obtained from the Span and Wagner EoS [41] were used as a reference densities to tune the unknown parameters, (M_0/L_{00}) and γ_T, in this model at the full range of pressures for each measured isotherm. The measurement procedure as well as the method to determine the combined standard uncertainties [42][43] for each measured density were well described in the authors' previous publication [36].

3. Specific heat capacity calculations

The residual specific heat capacity ($C_p - C_p^0$) can be calculated from the measured density data through the following equation [44]:

$$\rho = \left(\frac{\partial C_p}{\partial P}\right)_T = -T\left(\frac{\partial^2 v}{\partial T^2}\right)_P \quad (3)$$

In this equation, the gradient of molar volume with temperature at each constant pressure were plotted using the measured densities at the five measured isotherms. The procedure to calculate the specific heat capacity from Equation (3) has also been described in a previous publication for the CO_2-H_2S system [36]. A similar procedure was undertaken in this work. The constants B to F in the Aly & Lee equation [45] to calculate the ideal gas specific heat capacity, C_{pi}^0, for CO_2 and SO_2 components is summarised in Table 2. The obtained C_{pi}^0 from the Aly & Lee equation [45] is in $J.K^{-1}.kmol^{-1}$.

4. Results and discussions

Densities of CO_2-SO_2 binary systems were measured using vibrating tube densitometer (VTD), Anton Paar DMA 512 in the gas, liquid and supercritical phases at pressures up to 41.7 MPa. The composition of the binary system was 0.9478 CO_2 + 0.0522 SO_2 at 298 K and 0.9503 CO_2 + 0.0497 SO_2 at 273, 283, 323 and 353 K. At each isotherm, the densitometer was firstly calibrated using pure CO_2 with a forced path mechanical calibration (FPMC) technique [38]. The measured densities along with their uncertainties and compressibility factor at each corresponding pressure, temperature and phase are reported in Tables 3 through 7 for each isotherm. The uncertainty values in the gas, liquid and supercritical phases are summarised for each isotherm in Table 8. The measured densities then are compared against various equations of state including Soave-Redlich-Kwong [26] (SRK), Peng-Robinson [27] (PR), Patel-Teja [29] with Valderrama modification [28] (VPT), those with introducing CO_2

volume fraction [30][46] and Peneloux shift parameter [31] as well as multi parameter equation of state based on Helmholtz energy [33]. In this work, the modified binary interaction parameter, k_{ij} or *BIP*, for the CO_2-SO_2 was 0.02 for all cubic EoSs. The Average Absolute Deviation (AAD) of these model predictions from the obtained density data was calculated from the following equation:

$$AAD\ (\%) = N^{-1} \sum_{i=1}^{N} \left(\left| \rho_{Exp.} - \rho_{Model} \right| / \rho_{Exp.} \right) \times 100 \qquad (4)$$

Table 9 summarises the AAD and Maximum Absolute Deviation (MAD) of the investigated EoSs in the gas, liquid and supercritical phases as well as the overall quantities. Thermodynamic properties of the investigated mixtures, i.e., compressibility factor, isobaric specific heat capacity and bubble points, were derived from the measured densities. Table 10 gives the derived specific heat capacities of the binary system and predicted quantities with the multi parameter EoS. The bubble points of the mixture are summarised at two isotherms in Table 11.

The measured densities, as shown in Table 3 to 7, varies over a wide range from 1.0 kg/m^3 at 297.42 k and 0.051 MPa to 1110.7 kg/m^3 at 273.54 K and 41.723 MPa. Overall (see Table 8), 454 density data were obtained of which 97 points were in the gas phase, 221 points in the liquid phase and 136 points in the supercritical phase. Figure 2 demonstrates the measured and predicted densities using multi parameter EoS at different isotherms. Values at lower pressures, i.e. pressures less than 8 MPa and densities below 200 kg/m^3 are shown in Figure 3.

The maximum uncertainty of the measured densities [42][43], as shown in Table 8, is $u_r(\rho)$ = 4.4% in the gas phase at 298 K and very low pressure conditions. However, the average uncertainty in the gas phase at all isotherms is $u_r(\rho)$ = 0.6%. The average uncertainty in the liquid phase is also $u_r(\rho)$ = 0.03% with the maximum value of $u_r(\rho)$ = 1.0%. Those in the supercritical phase is $u_r(\rho)$ = 0.1% and $u_r(\rho)$ = 1.0% for the average and maximum uncertainties, respectively. Overall, the average uncertainty for the measured densities is $u(\rho)$ = 0.4 kg/m^3 or $u_r(\rho)$ = 0.2% with the maximum value of $u(\rho)$ = 2.7 kg/m^3 or $u_r(\rho)$ = 4.4%.

The measured densities using VTD densitometer with the FPMC calibration procedure in this work, were already validated in the authors' previous publication [36] for the CO_2-H_2S

system by comparing the measured values of CO_2-H_2S to the data published by Stouffer et al. [47][48] at two isotherms.

The measured densities were employed to evaluate accuracy of various equations of state in this work. As summarised in Table 9, first the classical cubic EoSs were tested. The AAD for the SRK-EoS in the gas, liquid and supercritical phases is 2.4%, 8.2% and 9.6% with an overall AAD of 7.4% and MAD of 15.2%. Those for the PR-EoS was 1.8%, 3.2% and 2.4% with an overall AAD of 2.6% and MAD of 7.6%. The AAD for the VPT-EoS is 1.8%, 1.9% and 2.6% in the gas, liquid and supercritical phases with an overall AAD of 2.1%. The most accurate EoS in the gas phase is VPT and PR EoSs with an AAD of 1.8%, VPT-EoS in the liquid phase with the AAD of 1.9% and PR-EoS in the supercritical phase with the AAD of 2.4%. However, the VPT-EoS is the most accurate among them with the overall AAD of 2.1% and MAD of 8.0%.

Introducing the CO_2 correction term [30][46] to the above EoSs then could significantly improve their prediction accuracy for the densities of the investigated binary system. The overall AAD of SRK-CO_2 and PR-CO_2 EoSs is 1.0% (reduced from 7.4% and 2.6% to 1.0%) which are the most accurate EoSs with the CO_2 volume correction term. The MAD for these are 8.0 and 7.4%, respectively. PR-CO_2 in the gas phase (with the AAD of 1.7%) and SRK-CO_2 in the liquid and supercritical phases (with the AAD of 0.6% and 0.8%) are the most accurate EoS in the different phases. In addition to the CO_2 volume correction term, the Peneloux shift parameter also was introduced to the SRK and PR EoSs. This could also reduce the overall AAD to 2.6% and 2.1% for the SRK and PR EoSs, respectively. Among all classical cubic EoSs, the PR-CO_2 with the AAD and MAD of 1.0% and 7.4% is the most accurate EoS for the investigated mixture.

Apart from classical cubic EoSs, the multi parameter EoS also were evaluated using the measured densities. As shown in Table 9, the multi parameter EoS predicts the densities more accurately compared to the classical EoSs. The AAD of multi parameter EoS from the measured densities in the gas, liquid and supercritical phases are 1.6%, 0.2% and 0.6% with the overall AAD and MAD of 0.6% and 8.0%. Figure 4 shows the deviations of the multi parameter EoS from the measured densities.

The compressibility factor of the investigated mixture were derived from the measured densities, which were reported in Tables 3 to 7. Figures 5 and 6 show the derived z-factors at

all pressure ranges and at pressures lower than 10 MPa, respectively. The lines in these figures demonstrate the predicted z-factors using the multi parameter EoS at each isotherms. As can be seen, they are in good agreement and the AAD of the multi parameter EoS from the derived z-factors is 1.6%, 0.2% and 0.6% in the gas, liquid and supercritical phases. The overall AAD is also 0.6%.

The isobaric specific heat capacities were calculated from thermodynamic equations and using the measured densities at various pressure and temperature. The C_p were calculated at the constant pressures of 15, 20, 25, 30, 35 and 40 MPa using Equation (3). The measured specific heat capacities were compared against the predictions using the multi parameter EoS. As shown in Table 10, the AAD of the multi parameter EoS from the derived values is 5.8% which shows the model predictions and the experimentally derived values are in the good agreement. Figure 7 also shows the determined specific heat capacities at different pressures. The lines in the figure show the predicted specific heat capacities using the multi parameter EoS. However, it is suggested that these values should be compared to the directly measured heat capacities, e.g., measured C_p using adapted calorimeters.

The procedure of conducting the tests in each isotherm was injecting the sample fluid at a very slow rate to reach the dew point and continuing on the injection to reach the bubble point and further injection to achieve the desired pressure. Continuous data recording during the test, particularly in the vicinity of the dew and bubble points, allows fitting the representative correlation to the experimental data on each side of the dew or bubble point. Therefore, the precise location of the dew or bubble point could be determined by crossing the fitted correlations. The calculated bubble points at two isotherms of 273 K and 283 K as well as the predicted amounts using PR-CO_2 EoS were summarised in Table 11. An overall AAD of 3.6% was achieved by comparing the measured and predicted values. Figures 8 shows the bubble point measurements. The circle points in this figure show the cross points of the fitted correlations which correspond to the dew or bubble points. The conclusion of this comparison is that the densitometer is not very accurate for estimation of bubble and dew point pressure. In comparison with VLE prediction using PR-CO_2 EoS, there is a difference of at least 0.1MPa, which is higher than experimental uncertainty of pressure using the static analytical method [25].

5. Conclusion

The densities of CO_2-SO_2 binary mixture were measured using VTD densitometer, Anton Paar DMA 512, in the gas, liquid and supercritical phases. The densitometer was first calibrated using pure CO_2 and the FPMC calibration technique. Then, the densities of a 0.9503 CO_2 – 0.0497 SO_2 mixture were measured at temperatures of 273, 283, 323 and 353 K. In addition the densities of 0.9478 CO_2 – 0.0522 SO_2 were measured at 298 K. The overall average uncertainty of the measured densities with a confidence level of 95% was $u_r(\rho)$ = 0.2% or $u(\rho)$ = 0.4 kg/m^3. The highest uncertainties were observed at very low pressure conditions in the gas phase or in the vicinity of the bubble point curve in the liquid phase. The measured densities were employed to evaluate classical cubic EoSs, those with CO_2 volume correction term and Peneloux shift parameter as well as the multi parameter EoS. Among the classical EoSs, the PR-CO_2 was the most accurate EoS for the investigated mixture with an AAD of 1.0% and MAD of 7.4%. However, the multi parameter EoS was the most accurate EoS with an AAD of only 0.6% and MAD of 8.0%. From the measured densities for the CO_2-SO_2 system, the thermodynamic properties were derived and compared to the EoSs. The compressibility factor was in a good agreement with the multi parameter EoS with an AAD of 0.6%. The isobaric specific heat capacity was derived from thermodynamic equations and measured densities. The AAD of the predicted specific heat capacity using the multi parameter EoS from the derived quantities was 5.8%. The bubble points at two different isotherms of 273 and 283 K were measured by fitting the equations to the numerous measured densities on both sides of bubble points. The AAD of the predicted bubble points using PR-CO_2 EoS from the measured values was 3.6%.

6. Acknowledgements

This work was a part of the JIP project" Impact of Common Impurities on Carbon Dioxide Capture, Transport and Storage" [30] which the phase-I was conducted jointly at Heriot-Watt University in Edinburgh, UK and MINES ParisTech in France in 2011-2014. The authors would like to gratefully acknowledge the sponsors of the project: Chevron, GALP Energia, Linde AG Engineering Division, OMV, Petroleum Expert, Statoil, TOTAL and National Grid Carbon Ltd. The thermophysical properties of CO_2-rich fluids where investigated during the course of project are phase equilibira, hydrates [49], solid formation, density [36][46][50], viscosity, interfacial tension [51], solubility [52][53][54] and pH.

REFERENCES

[1] D. Y. C. Leung, G. Caramanna, and M. M. Maroto-Valer, "An overview of current status of carbon dioxide capture and storage technologies," *Renew. Sustain. Energy Rev.*, vol. 39, pp. 426–443, 2014.

[2] J.-Y. Lee, T. C. Keener, and Y. J. Yang, "Potential Flue Gas Impurities in Carbon Dioxide Streams Separated from Coal-Fired Power Plants," *J. Air Waste Manage. Assoc.*, vol. 59, no. 6, pp. 725–732, Feb. 2012.

[3] R. T. J. Porter, M. Fairweather, M. Pourkashanian, and R. M. Woolley, "The range and level of impurities in CO2 streams from different carbon capture sources," *Int. J. Greenh. Gas Control*, vol. 36, pp. 161–174, May 2015.

[4] F. Farelas, Y. S. Choi, and S. Nešić, "Corrosion Behavior of API 5L X65 Carbon Steel Under Supercritical and Liquid Carbon Dioxide Phases in the Presence of Water and Sulfur Dioxide," *Corrosion*, vol. 69, no. 3, pp. 243–250, Mar. 2013.

[5] D. Liu, T. Wall, and R. Stanger, "CO2 quality control in Oxy-fuel technology for CCS: SO2 removal by the caustic scrubber in Callide Oxy-fuel Project," *Int. J. Greenh. Gas Control*, vol. 51, pp. 207–217, 2016.

[6] A. Kather and S. Kownatzki, "Assessment of the different parameters affecting the CO2 purity from coal fired oxyfuel process," *Int. J. Greenh. Gas Control*, vol. 5, pp. S204–S209, Jun. 2011.

[7] M. Woods and M. Matuszewski, "Quality Guideline for Energy System Studies: CO2 Impurity Design Parameters, NETL/DOE-341/011212, 2013."

[8] K. Stéphenne, "Start-up of World's First Commercial Post-combustion Coal Fired CCS Project: Contribution of Shell Cansolv to SaskPower Boundary Dam ICCS Project," *Energy Procedia*, vol. 63, pp. 6106–6110, 2014.

[9] S. Bachu and W. D. Gunter, "Overview of acid-gas injection operations in western Canada," *Proc. 7th Int. Conf. Greenh. Gas Control Technol. vol. 1. Peer-Reviewed Pap. Plenary Present. IEA Greenh. Gas R&D Program. Cheltenham, UK*, 2005.

[10] A. Battistelli, P. Ceragioli, and M. Marcolini, "Injection of Acid Gas Mixtures in Sour Oil Reservoirs: Analysis of Near-Wellbore Processes with Coupled Modelling of Well and Reservoir Flow," *Transp. Porous Media*, vol. 90, no. 1, pp. 233–251, Nov. 2010.

[11] Z. Wang, J. Wang, C. Lan, I. He, V. Ko, D. Ryan, and A. Wigston, "A study on the impact of SO2 on CO2 injectivity for CO2 storage in a Canadian saline aquifer," *Appl. Energy*, vol. 184, pp. 329–336, 2016.

[12] Q. Li, X. Li, N. Wei, and Z. Fang, "Possibilities and potentials of geological co-storage CO2 and SO2 in China," *Energy Procedia*, vol. 4, pp. 6015–6020, 2011.

[13] R. Miri, P. Aagaard, and H. Hellevang, "Examination of CO2 - SO2 Solubility in Water by SAFT1. Implications for CO2 Transport and Storage," *J. Phys. Chem. B*, vol. 118, no. 34, pp. 10214–10223, Aug. 2014.

[14] J. Zhu and D. Harris, "Modeling potential impacts of SO2 co-injected with CO2 on the Knox Group, western Kentucky | American Geosciences Institute," 2016.

[15] Z. Ziabakhsh-Ganji and H. Kooi, "Sensitivity of the CO2 storage capacity of underground geological structures to the presence of SO2 and other impurities," *Appl. Energy*, vol. 135, pp. 43–52, 2014.

[16] J. K. Pearce, G. K. W. Dawson, A. C. K. Law, D. Biddle, and S. D. Golding, "Reactivity of micas and cap-rock in wet supercritical CO2 with SO2 and O2 at CO2 storage conditions," *Appl. Geochemistry*, vol. 72, pp. 59–76, 2016.

[17] S. García, Q. Liu, and M. M. Maroto-Valer, "A novel high pressure-high temperature experimental apparatus to study sequestration of CO2 - SO2 mixtures in geological formations," *Greenh. Gases Sci. Technol.*, vol. 4, no. 4, pp. 544–554, Aug. 2014.

[18] IEAGHG, "Effects of Impurities on Geological Storage of CO2, Report 2011/04," 2011.

[19] S. P. Tan, Y. Yao, and M. Piri, "Modeling the Solubility of SO2 + CO2 Mixtures in Brine at Elevated Pressures and Temperatures," *Ind. Eng. Chem. Res.*, vol. 52, no. 31, pp. 10864–10872, Aug. 2013.

[20] S. Waldmann and H. Rütters, "Geochemical effects of SO2 during CO2 storage in deep saline reservoir sandstones of Permian age (Rotliegend) – A modeling approach," *Int. J. Greenh. Gas Control*, vol. 46, pp. 116–135, 2016.

[21] E. Hendriks, G. M. Kontogeorgis, R. Dohrn, J.-C. de Hemptinne, I. G. Economou, L. F. Žilnik, and V. Vesovic, "Industrial Requirements for Thermodynamics and Transport Properties," *Ind. Eng. Chem. Res.*, vol. 49, no. 22, pp. 11131–11141, Nov. 2010.

[22] H. Li, J. P. Jakobsen, Ø. Wilhelmsen, and J. Yan, "PVTxy properties of CO2 mixtures relevant for CO2 capture, transport and storage: Review of available experimental data and theoretical models," *Appl. Energy*, vol. 88, no. 11, pp. 3567–3579, Nov. 2011.

[23] M. F. Caubet, "Liquéfaction des mélanges gazeux. Université de Bordeaux Thesis." 1901.

[24] V. Lachet, T. de Bruin, P. Ungerer, C. Coquelet, A. Valtz, V. Hasanov, F. Lockwood, and D. Richon, "Thermodynamic behavior of the CO2+SO2 mixture: Experimental and Monte Carlo simulation studies," *Energy Procedia*, vol. 1, no. 1, pp. 1641–1647, Feb. 2009.

[25] C. Coquelet, A. Valtz, and P. Arpentinier, "Thermodynamic study of binary and ternary systems containing CO2+impurities in the context of CO2 transportation," *Fluid Phase Equilib.*, vol. 382, pp. 205–211, Nov. 2014.

[26] G. Soave, "Equilibrium constants from a modified Redlich-Kwong equation of state," *Chem. Eng. Sci.*, vol. 27, no. 6, pp. 1197–1203, Jun. 1972.

[27] D.-Y. Peng and D. B. Robinson, "A New Two-Constant Equation of State," *Ind. Eng. Chem. Fundam.*, vol. 15, no. 1, pp. 59–64, Feb. 1976.

[28] J. O. Valderrama, "A generalized Patel-Teja equation of state for polar and nonpolar fluids and their mixtures.," *J. Chem. Eng. JAPAN*, vol. 23, no. 1, pp. 87–91, Mar. 1990.

[29] N. C. Patel and A. S. Teja, "A new cubic equation of state for fluids and fluid mixtures," *Chem. Eng. Sci.*, vol. 37, no. 3, pp. 463–473, 1982.

[30] A. Chapoy, M. Nazeri, M. Kapateh, R. Burgass, C. Coquelet, and B. Tohidi, "Effect of impurities on thermophysical properties and phase behaviour of a CO2-rich system in CCS," *Int. J. Greenh. Gas Control*, vol. 19, pp. 92–100, Nov. 2013.

[31] A. Péneloux, E. Rauzy, and R. Fréze, "A consistent correction for Redlich-Kwong-Soave volumes," *Fluid Phase Equilib.*, vol. 8, no. 1, pp. 7–23, Jan. 1982.

[32] O. Kunz and W. Wagner, “The GERG-2008 Wide-Range Equation of State for Natural Gases and Other Mixtures: An Expansion of GERG-2004,” *J. Chem. Eng. Data*, vol. 57, no. 11, pp. 3032–3091, Nov. 2012.

[33] J. Gernert and R. Span, “EOS–CG: A Helmholtz energy mixture model for humid gases and CCS mixtures,” *J. Chem. Thermodyn.*, vol. 93, pp. 274–293, 2016.

[34] E. W. Lemmon and R. Span, “Short Fundamental Equations of State for 20 Industrial Fluids,” 2006.

[35] R. Span and W. Wagner, “A New Equation of State for Carbon Dioxide Covering the Fluid Region from the Triple-Point Temperature to 1100 K at Pressures up to 800 MPa,” *J. Phys. Chem. Ref. Data*, vol. 25, no. 6, pp. 1509–1596, Nov. 1996.

[36] M. Nazeri, A. Chapoy, A. Valtz, C. Coquelet, and B. Tohidi, “Densities and derived thermophysical properties of the 0.9505 CO2+0.0495 H2S mixture from 273 K to 353 K and pressures up to 41 MPa,” *Fluid Phase Equilib.*, vol. 423, pp. 156–171, Sep. 2016.

[37] C. Coquelet, D. Ramjugernath, H. Madani, A. Valtz, P. Naidoo, and A. H. Meniai, “Experimental Measurement of Vapor Pressures and Densities of Pure Hexafluoropropylene,” *J. Chem. Eng. Data*, vol. 55, no. 6, pp. 2093–2099, Jun. 2010.

[38] C. Bouchot and D. Richon, “An enhanced method to calibrate vibrating tube densimeters,” *Fluid Phase Equilib.*, vol. 191, no. 1–2, pp. 189–208, Nov. 2001.

[39] W. Khalil, C. Coquelet, and D. Richon, “High-Pressure Vapor−Liquid Equilibria, Liquid Densities, and Excess Molar Volumes for the Carbon Dioxide + 2-Propanol System from (308.10 to 348.00) K,” *J. Chem. Eng. Data*, vol. 52, no. 5, pp. 2032–2040, Sep. 2007.

[40] C. Bouchot and D. Richon, “Direct Pressure−Volume−Temperature and Vapor−Liquid Equilibrium Measurements with a Single Equipment Using a Vibrating Tube Densimeter up to 393 K and 40 MPa: Description of the Original Apparatus and New Data,” *Ind. Eng. Chem. Res.*, vol. 37, no. 8, pp. 3295–3304, Aug. 1998.

[41] R. Span and W. Wagner, “A New Equation of State for Carbon Dioxide Covering the Fluid Region from the Triple-Point Temperature to 1100 K at Pressures up to 800 MPa,” *J. Phys. Chem. Ref. Data*, vol. 25, no. 6, pp. 1509–1596, Nov. 1996.

[42] S. Bell, *Measurement Good Practice Guide No. 11 (Issue 2), A Beginner’s Guide to Uncertainty of Measurement*. National Physical Laboratory, 2001.

[43] B. N. Taylor and C. E. Kuyatt, *Guidelines for Evaluating and Expressing the Uncertainty of NIST Measurement Results*. NIST, 1994.

[44] J. J. Segovia, D. Vega-Maza, C. R. Chamorro, and M. C. Martín, “High-pressure isobaric heat capacities using a new flow calorimeter,” *J. Supercrit. Fluids*, vol. 46, no. 3, pp. 258–264, Oct. 2008.

[45] F. A. Aly and L. L. Lee, “Self-consistent equations for calculating the ideal gas heat capacity, enthalpy, and entropy,” *Fluid Phase Equilib.*, vol. 6, no. 3–4, pp. 169–179, Jan. 1981.

[46] M. Nazeri, A. Chapoy, R. Burgass, and B. Tohidi, “Measured densities and derived thermodynamic properties of CO2-rich mixtures in gas, liquid and supercritical phases from 273K to 423K and pressures up to 126MPa,” *J. Chem. Thermodyn.*, vol. 111, pp. 157–172, 2017.

[47] S. J. Kellerman, C. E. Stouffer, P. T. Eubank, J. C. Holste, and K. R. Hall,

"Thermodynamic Properties of CO2 + H2S Mixtures, GPA Research Report No. 143, prepared as part of GPA Project 842," *Ga Process. Assoc.*, 1995.

[48] C. E. Stouffer, S. J. Kellerman, K. R. Hall, J. C. Holste, B. E. Gammon, and K. N. Marsh, "Densities of Carbon Dioxide + Hydrogen Sulfide Mixtures from 220 K to 450 K at Pressures up to 25 MPa," *J. Chem. Eng. Data*, vol. 46, no. 5, pp. 1309–1318, Sep. 2001.

[49] A. Chapoy, R. Burgass, B. Tohidi, and I. Alsiyabi, "Hydrate and Phase Behavior Modeling in CO2-Rich Pipelines," *J. Chem. Eng. Data*, vol. 60, no. 2, pp. 447–453, Feb. 2015.

[50] A. G. Perez, A. Valtz, C. Coquelet, P. Paricaud, and A. Chapoy, "Experimental and modelling study of the densities of the hydrogen sulphide + methane mixtures at 253, 273 and 293 K and pressures up to 30 MPa," *Fluid Phase Equilib.*, vol. 427, pp. 371–383, 2016.

[51] L. M. C. Pereira, A. Chapoy, R. Burgass, and B. Tohidi, "Measurement and modelling of high pressure density and interfacial tension of (gas+n-alkane) binary mixtures," *J. Chem. Thermodyn.*, vol. 97, pp. 55–69, 2016.

[52] M. H. Kapateh, A. Chapoy, R. Burgass, and B. Tohidi, "Experimental Measurement and Modeling of the Solubility of Methane in Methanol and Ethanol," *J. Chem. Eng. Data*, vol. 61, no. 1, pp. 666–673, Jan. 2016.

[53] M. Wise, A. Chapoy, and R. Burgass, "Solubility Measurement and Modeling of Methane in Methanol and Ethanol Aqueous Solutions," *J. Chem. Eng. Data*, vol. 61, no. 9, pp. 3200–3207, Sep. 2016.

[54] M. Wise and A. Chapoy, "Carbon dioxide solubility in Triethylene Glycol and aqueous solutions," *Fluid Phase Equilib.*, vol. 419, pp. 39–49, 2016.

[55] R. Span and W. Wagner, "Equations of State for Technical Applications. I. Simultaneously Optimized Functional Forms for Nonpolar and Polar Fluids," *Int. J. Thermophys.*, vol. 24, no. 1, pp. 1–39.

[56] R. Span and W. Wagner, "Equations of State for Technical Applications. II. Results for Nonpolar Fluids," *Int. J. Thermophys.*, vol. 24, no. 1, pp. 41–109, 2003.

[57] R. Span and W. Wagner, "Equations of State for Technical Applications. III. Results for Polar Fluids," *Int. J. Thermophys.*, vol. 24, no. 1, pp. 111–162, 2003.

[58] E. W. Lemmon and R. Tillner-Roth, "A Helmholtz energy equation of state for calculating the thermodynamic properties of fluid mixtures," *Fluid Phase Equilib.*, vol. 165, no. 1, pp. 1–21, Nov. 1999.

[59] E. W. Lemmon and R. T. Jacobsen, "A Generalized Model for the Thermodynamic Properties of Mixtures," *Int. J. Thermophys.*, vol. 20, no. 3, pp. 825–835, 1999.

Table 1 - Details of the chemicals, suppliers and purities of the components used in this study.

Chemical Name	Source	Initial Purity [a]	Certification	Analysis Method [b]
SO_2	Air Liquide	0.995 vol	Air Liquide Certified	SM
CO_2	Air Liquide	0.99995 vol	Air Liquide Certified	SM

[a] No additional purification is carried out for all samples.
[b] SM: Supplier method

Table 2 - Constants B to F in the Aly & Lee equation [45]

C_{pi} constants	*B*	*C*	*D*	*E*	*F*
CO_2	29400	34500	-1430	26400	588
SO_2	33400	25900	933	10900	424

Table 3 - Experimental results of the 0.9503 mole CO_2 + 0.0497 mole SO_2 system at 273 K [a]

No	Phase	*T*/K	*p*/MPa	*ρ*/kg.m^{-3}		*Z*	No	Phase	*T*/K	*p*/MPa	*ρ*/kg.m^{-3}		*Z*
				Exp.	$u_c(\rho)$						*Exp.*	$u_c(\rho)$	
1	Gas	272.65	0.226	4.8	0.1	0.93	44	Liquid	273.55	25.039	1063.6	0.3	0.47
2	Gas	272.65	0.407	8.5	0.1	0.95	45	Liquid	273.55	24.523	1061.9	0.2	0.46
3	Gas	272.65	0.503	10.6	0.1	0.94	46	Liquid	273.55	24.032	1060.4	0.3	0.45
4	Gas	272.65	0.752	16.2	0.1	0.92	47	Liquid	273.56	23.496	1058.4	0.3	0.44
5	Gas	272.65	1.013	22.1	0.1	0.91	48	Liquid	273.57	23.015	1056.6	0.3	0.43
6	Gas	272.65	1.252	27.9	0.1	0.89	49	Liquid	273.56	22.501	1054.9	0.2	0.42
7	Gas	272.65	1.506	34.4	0.1	0.87	50	Liquid	273.56	21.993	1053.0	0.3	0.41
8	Gas	272.65	1.752	40.9	0.2	0.85	51	Liquid	273.56	21.519	1051.3	0.3	0.41
9	Gas	272.65	1.998	47.9	0.2	0.83	52	Liquid	273.56	21.029	1049.7	0.3	0.40
10	Liquid	273.54	41.723	1110.7	0.2	0.74	53	Liquid	273.55	20.535	1047.9	0.2	0.39
11	Liquid	273.56	41.601	1110.4	0.2	0.74	54	Liquid	273.56	20.028	1046.0	0.3	0.38
12	Liquid	273.55	41.016	1109.0	0.2	0.73	55	Liquid	273.56	19.509	1044.0	0.2	0.37
13	Liquid	273.55	40.508	1107.8	0.2	0.72	56	Liquid	273.56	19.000	1042.1	0.3	0.36
14	Liquid	273.55	40.023	1106.6	0.1	0.72	57	Liquid	273.56	18.515	1040.1	0.3	0.35
15	Liquid	273.55	39.553	1105.7	0.2	0.71	58	Liquid	273.56	18.049	1038.2	0.3	0.34
16	Liquid	273.55	38.992	1104.0	0.2	0.70	59	Liquid	273.56	17.514	1036.2	0.3	0.33
17	Liquid	273.54	38.558	1103.1	0.2	0.69	60	Liquid	273.57	17.024	1034.2	0.3	0.33
18	Liquid	273.54	38.033	1101.8	0.2	0.68	61	Liquid	273.57	16.500	1031.9	0.3	0.32
19	Liquid	273.54	37.529	1100.5	0.2	0.67	62	Liquid	273.57	15.999	1029.8	0.3	0.31
20	Liquid	273.54	37.047	1099.0	0.2	0.67	63	Liquid	273.58	15.602	1028.1	0.3	0.30
21	Liquid	273.54	36.490	1097.6	0.2	0.66	64	Liquid	273.57	14.951	1025.4	0.3	0.29
22	Liquid	273.54	36.045	1096.7	0.2	0.65	65	Liquid	273.57	14.518	1023.6	0.3	0.28
23	Liquid	273.54	35.534	1095.1	0.2	0.64	66	Liquid	273.56	23.496	1058.4	0.3	0.44
24	Liquid	273.54	35.043	1093.9	0.3	0.63	67	Liquid	273.56	13.506	1019.3	0.3	0.26
25	Liquid	273.54	34.491	1092.3	0.2	0.62	68	Liquid	273.56	13.012	1017.2	0.3	0.25
26	Liquid	273.54	34.032	1091.1	0.2	0.62	69	Liquid	273.56	12.509	1014.7	0.3	0.24
27	Liquid	273.54	33.521	1089.7	0.2	0.61	70	Liquid	273.57	12.005	1012.2	0.3	0.23
28	Liquid	273.54	33.027	1088.3	0.2	0.60	71	Liquid	273.57	11.502	1009.5	0.3	0.23
29	Liquid	273.54	32.491	1086.7	0.3	0.59	72	Liquid	273.57	11.003	1007.0	0.3	0.22
30	Liquid	273.54	31.975	1085.1	0.2	0.58	73	Liquid	273.57	10.516	1004.5	0.4	0.21
31	Liquid	273.55	31.482	1083.6	0.2	0.57	74	Liquid	273.57	9.944	1001.9	0.3	0.20
32	Liquid	273.55	30.952	1082.2	0.2	0.57	75	Liquid	273.58	9.518	999.7	0.4	0.19
33	Liquid	273.54	30.524	1080.9	0.2	0.56	76	Liquid	273.58	9.008	996.7	0.4	0.18
34	Liquid	273.55	30.026	1079.4	0.3	0.55	77	Liquid	273.58	8.503	993.8	0.4	0.17
35	Liquid	273.54	29.514	1077.7	0.2	0.54	78	Liquid	273.60	8.003	990.6	0.4	0.16
36	Liquid	273.54	29.024	1076.3	0.2	0.53	79	Liquid	273.60	7.688	987.5	0.4	0.15
37	Liquid	273.55	28.539	1074.9	0.2	0.53	80	Liquid	273.60	7.034	984.6	0.4	0.14
38	Liquid	273.55	28.041	1073.0	0.3	0.52	81	Liquid	273.60	6.503	981.9	0.4	0.13
39	Liquid	273.55	27.554	1071.7	0.2	0.51	82	Liquid	273.60	6.005	978.7	0.4	0.12
40	Liquid	273.54	26.999	1069.9	0.2	0.50	83	Liquid	273.60	5.521	975.5	0.4	0.11
41	Liquid	273.55	26.484	1068.3	0.2	0.49	84	Liquid	273.61	5.013	972.1	0.4	0.10
42	Liquid	273.55	26.016	1066.9	0.3	0.48	85	Liquid	273.61	4.518	968.2	0.4	0.09
43	Liquid	273.54	25.506	1065.1	0.2	0.47	86	Liquid	273.60	4.001	964.9	0.5	0.08

[a] Standard uncertainties, *u*, are $u(T)$ = 0.02 K, $u(p)$ = 0.002 MPa for pressures up to 10 MPa and $u(p)$ = 0.005 MPa for pressures from 10-40 MPa, for SO_2 $u(z)$ = 0.0001 and for CO_2 $u(z)$ = 0.0018

Table 4 - Experimental results of the 0.9503 mole CO_2 + 0.0497 mole SO_2 system at 283 K [a]

No	Phase	*T*/K	*p*/MPa	*ρ*/kg.m^{-3}		*Z*	No	Phase	*T*/K	*p*/MPa	*ρ*/kg.m^{-3}		*Z*
				Exp.	$u_c(\rho)$						*Exp.*	$u_c(\rho)$	
1	Gas	282.66	0.120	2.5	0.1	0.92	48	Liquid	283.32	26.503	1034.9	0.3	0.49
2	Gas	282.66	0.211	4.3	0.1	0.94	49	Liquid	283.32	26.038	1033.5	0.2	0.48
3	Gas	282.66	0.301	6.1	0.1	0.94	50	Liquid	283.32	25.509	1031.3	0.3	0.47
4	Gas	282.66	0.408	8.5	0.1	0.92	51	Liquid	283.32	25.025	1029.4	0.3	0.46
5	Gas	282.66	0.511	10.6	0.1	0.92	52	Liquid	283.32	24.535	1027.4	0.3	0.46
6	Gas	282.66	0.608	12.3	0.1	0.95	53	Liquid	283.33	24.074	1025.3	0.2	0.45
7	Gas	282.65	0.800	16.5	0.1	0.93	54	Liquid	283.32	23.509	1023.3	0.2	0.44
8	Gas	282.66	1.009	21.1	0.1	0.92	55	Liquid	283.32	23.052	1021.8	0.3	0.43
9	Gas	282.65	1.249	26.3	0.1	0.91	56	Liquid	283.32	22.565	1019.8	0.3	0.42
10	Gas	282.66	1.509	32.8	0.1	0.88	57	Liquid	283.32	22.046	1017.6	0.2	0.41
11	Gas	282.66	1.705	37.5	0.1	0.87	58	Liquid	283.32	21.504	1015.3	0.3	0.40
12	Gas	282.66	1.909	42.7	0.1	0.86	59	Liquid	283.32	21.035	1013.2	0.2	0.40
13	Gas	282.66	2.010	45.2	0.1	0.85	60	Liquid	283.32	20.507	1011.0	0.3	0.39
14	Gas	282.66	2.199	50.5	0.2	0.83	61	Liquid	283.32	20.038	1008.7	0.3	0.38
15	Gas	282.66	2.508	59.6	0.2	0.81	62	Liquid	283.32	19.496	1006.2	0.3	0.37
16	Gas	282.66	2.702	65.5	0.2	0.79	63	Liquid	283.32	19.016	1004.1	0.3	0.36
17	Gas	282.66	3.008	76.0	0.2	0.76	64	Liquid	283.32	18.520	1001.7	0.3	0.35
18	Liquid	283.32	40.729	1080.4	0.2	0.72	65	Liquid	283.33	18.078	999.5	0.3	0.35
19	Liquid	283.33	40.700	1080.6	0.2	0.72	66	Liquid	283.32	17.551	996.8	0.3	0.34
20	Liquid	283.33	40.601	1080.3	0.2	0.72	67	Liquid	283.32	17.047	994.7	0.3	0.33
21	Liquid	283.33	40.145	1078.8	0.2	0.71	68	Liquid	283.32	16.561	992.4	0.3	0.32
22	Liquid	283.32	39.558	1077.4	0.2	0.70	69	Liquid	283.32	16.044	989.5	0.3	0.31
23	Liquid	283.32	39.056	1076.1	0.2	0.69	70	Liquid	283.32	15.505	986.8	0.4	0.30
24	Liquid	283.32	38.461	1074.6	0.2	0.68	71	Liquid	283.32	15.011	984.1	0.3	0.29
25	Liquid	283.31	38.061	1073.3	0.2	0.68	72	Liquid	283.32	14.496	980.8	0.4	0.28
26	Liquid	283.31	37.578	1072.1	0.2	0.67	73	Liquid	283.33	14.003	978.2	0.4	0.27
27	Liquid	283.32	37.026	1070.5	0.2	0.66	74	Liquid	283.32	13.536	975.3	0.4	0.27
28	Liquid	283.31	36.515	1068.6	0.2	0.65	75	Liquid	283.32	13.000	972.6	0.4	0.26
29	Liquid	283.31	36.037	1067.5	0.2	0.64	76	Liquid	283.32	12.514	969.7	0.4	0.25
30	Liquid	283.31	35.516	1065.8	0.2	0.64	77	Liquid	283.32	12.009	966.2	0.4	0.24
31	Liquid	283.32	34.989	1064.3	0.2	0.63	78	Liquid	283.33	11.512	963.0	0.4	0.23
32	Liquid	283.31	34.500	1062.8	0.2	0.62	79	Liquid	283.32	11.007	959.9	0.4	0.22
33	Liquid	283.32	33.995	1060.8	0.2	0.61	80	Liquid	283.32	10.507	956.6	0.4	0.21
34	Liquid	283.32	33.527	1059.6	0.2	0.60	81	Liquid	283.32	9.995	953.3	0.4	0.20
35	Liquid	283.32	33.032	1057.9	0.2	0.60	82	Liquid	283.32	9.510	949.7	0.4	0.19
36	Liquid	283.32	32.516	1056.2	0.2	0.59	83	Liquid	283.33	9.019	946.2	0.4	0.18
37	Liquid	283.32	32.033	1054.6	0.3	0.58	84	Liquid	283.33	8.543	942.8	0.5	0.17
38	Liquid	283.32	31.500	1052.8	0.2	0.57	85	Liquid	283.32	8.008	938.7	0.5	0.16
39	Liquid	283.32	31.007	1050.9	0.3	0.56	86	Liquid	283.32	7.506	934.7	0.5	0.15
40	Liquid	283.32	30.506	1049.6	0.3	0.56	87	Liquid	283.32	7.000	929.5	0.5	0.14
41	Liquid	283.32	30.008	1047.3	0.3	0.55	88	Liquid	283.32	6.507	925.6	0.5	0.13
42	Liquid	283.32	29.470	1045.7	0.2	0.54	89	Liquid	283.32	6.002	920.8	0.5	0.12
43	Liquid	283.32	29.081	1044.1	0.3	0.53	90	Liquid	283.32	5.506	916.4	0.6	0.11
44	Liquid	283.32	28.527	1042.4	0.2	0.52	91	Liquid	283.32	5.005	910.4	0.6	0.11
45	Liquid	283.32	28.043	1040.7	0.2	0.51	92	Liquid	283.33	4.499	904.4	0.6	0.10
46	Liquid	283.31	27.537	1038.9	0.2	0.51	93	Liquid	283.33	4.307	902.3	0.6	0.09
47	Liquid	283.32	27.023	1037.0	0.2	0.50							

[a] Standard uncertainties, *u*, are $u(T)$ = 0.02 K, $u(p)$ = 0.002 MPa for pressures up to 10 MPa and $u(p)$ = 0.005 MPa for pressures from 10-40 MPa, for SO_2 $u(z)$ = 0.0001 and for CO_2 $u(z)$ = 0.0018

Table 5 - Experimental results of the 0.9478 mole CO_2 + 0.0522 mole SO_2 system at 298 K [a]

No	Phase	*T*/K	*p*/MPa	ρ/kg.m^{-3}		*Z*	No	Phase	*T*/K	*p*/MPa	ρ/kg.m^{-3}		*Z*
				Exp.	$u_c(\rho)$						*Exp.*	$u_c(\rho)$	
1	Gas	297.42	0.051	1.0	0.0	0.93	47	Liquid	298.11	28.987	993.1	0.3	0.53
2	Gas	297.41	0.100	1.8	0.1	1.01	48	Liquid	298.10	28.400	990.6	0.3	0.52
3	Gas	297.41	0.200	3.6	0.1	1.01	49	Liquid	298.10	27.973	988.6	0.3	0.51
4	Gas	297.42	0.397	7.5	0.1	0.96	50	Liquid	298.10	27.508	986.6	0.3	0.51
5	Gas	297.42	0.502	9.4	0.1	0.97	51	Liquid	298.10	27.025	984.3	0.3	0.50
6	Gas	297.42	1.817	37.6	0.1	0.88	52	Liquid	298.09	26.503	982.1	0.3	0.49
7	Gas	297.41	2.012	42.1	0.1	0.87	53	Liquid	298.09	26.076	980.0	0.3	0.48
8	Gas	297.41	2.215	47.2	0.1	0.86	54	Liquid	298.10	25.593	977.9	0.3	0.48
9	Gas	297.42	2.421	53.0	0.1	0.83	55	Liquid	298.10	25.050	975.1	0.3	0.47
10	Gas	297.42	2.588	57.0	0.1	0.83	56	Liquid	298.10	24.505	972.6	0.3	0.46
11	Gas	297.42	2.854	64.1	0.2	0.81	57	Liquid	298.10	24.029	970.2	0.3	0.45
12	Gas	297.44	3.064	70.1	0.2	0.80	58	Liquid	298.10	23.522	967.7	0.3	0.44
13	Gas	297.43	3.223	74.6	0.2	0.79	59	Liquid	298.11	23.041	965.2	0.3	0.43
14	Gas	297.43	3.396	79.8	0.2	0.78	60	Liquid	298.10	22.537	962.6	0.3	0.43
15	Gas	297.42	3.638	87.4	0.2	0.76	61	Liquid	298.10	21.994	959.8	0.3	0.42
16	Gas	297.42	3.822	93.7	0.2	0.74	62	Liquid	298.11	21.501	957.0	0.3	0.41
17	Gas	297.42	3.996	99.9	0.2	0.73	63	Liquid	298.10	21.016	954.5	0.4	0.40
18	Gas	297.43	4.206	107.7	0.2	0.71	64	Liquid	298.11	20.492	951.5	0.4	0.39
19	Gas	297.42	4.401	115.6	0.3	0.69	65	Liquid	298.11	20.051	948.9	0.4	0.38
20	Gas	297.42	4.507	120.1	0.3	0.68	66	Liquid	298.11	19.477	945.6	0.4	0.37
21	Gas	297.42	4.600	124.4	0.3	0.67	67	Liquid	298.11	19.025	942.9	0.4	0.37
22	Gas	297.42	4.703	129.2	0.3	0.66	68	Liquid	298.11	18.527	939.8	0.4	0.36
23	Gas	297.40	4.803	134.4	0.6	0.65	69	Liquid	298.11	17.978	936.5	0.4	0.35
24	Liquid	298.12	40.411	1032.1	0.2	0.71	70	Liquid	298.11	17.492	933.3	0.4	0.34
25	Liquid	298.11	40.060	1031.1	0.3	0.71	71	Liquid	298.11	17.024	930.2	0.4	0.33
26	Liquid	298.11	39.519	1029.5	0.2	0.70	72	Liquid	298.11	16.534	926.8	0.4	0.32
27	Liquid	298.11	38.913	1027.8	0.3	0.69	73	Liquid	298.11	16.016	923.0	0.4	0.32
28	Liquid	298.11	38.545	1026.6	0.3	0.68	74	Liquid	298.11	15.500	919.1	0.4	0.31
29	Liquid	298.11	37.960	1024.8	0.2	0.67	75	Liquid	298.11	15.011	915.2	0.4	0.30
30	Liquid	298.11	37.574	1023.6	0.2	0.67	76	Liquid	298.12	14.500	910.9	0.5	0.29
31	Liquid	298.10	37.078	1022.0	0.2	0.66	77	Liquid	298.12	14.006	906.7	0.5	0.28
32	Liquid	298.10	36.493	1020.2	0.3	0.65	78	Liquid	298.11	13.500	902.3	0.5	0.27
33	Liquid	298.10	35.971	1018.4	0.2	0.64	79	Liquid	298.11	13.010	897.8	0.5	0.26
34	Liquid	298.11	35.494	1016.9	0.2	0.63	80	Liquid	298.12	12.503	892.9	0.5	0.25
35	Liquid	298.10	35.077	1015.5	0.2	0.63	81	Liquid	298.12	12.000	887.9	0.5	0.25
36	Liquid	298.10	34.441	1013.3	0.3	0.62	82	Liquid	298.12	11.504	882.9	0.5	0.24
37	Liquid	298.11	33.949	1011.6	0.2	0.61	83	Liquid	298.11	11.004	877.7	0.6	0.23
38	Liquid	298.10	33.435	1009.8	0.3	0.60	84	Liquid	298.11	10.505	872.1	0.6	0.22
39	Liquid	298.10	33.068	1008.6	0.2	0.60	85	Liquid	298.12	10.039	866.6	0.6	0.21
40	Liquid	298.10	32.518	1006.5	0.2	0.59	86	Liquid	298.12	9.508	860.5	0.6	0.20
41	Liquid	298.10	32.016	1004.6	0.2	0.58	87	Liquid	298.10	9.007	854.0	0.7	0.19
42	Liquid	298.11	31.516	1002.6	0.2	0.57	88	Liquid	298.11	8.501	846.7	0.7	0.18
43	Liquid	298.11	30.997	1000.7	0.2	0.56	89	Liquid	298.11	8.006	838.7	0.8	0.17
44	Liquid	298.11	30.505	998.9	0.3	0.56	90	Liquid	298.11	7.503	829.8	0.8	0.16
45	Liquid	298.11	30.013	996.8	0.3	0.55	91	Liquid	298.10	7.001	819.7	0.9	0.16
46	Liquid	298.11	29.543	994.8	0.3	0.54							

[a] Standard uncertainties, *u*, are $u(T)$ = 0.02 K, $u(p)$ = 0.002 MPa for pressures up to 10 MPa and $u(p)$ = 0.005 MPa for pressures from 10-40 MPa, for SO_2 $u(z)$ = 0.0001 and for CO_2 $u(z)$ = 0.0018

Table 6 - Experimental results of the 0.9503 mole CO_2 + 0.0497 mole SO_2 system at 323 K [a]

No	Phase	*T*/K	*p*/MPa	ρ/kg.m^{-3}		*Z*	No	Phase	*T*/K	*p*/MPa	ρ/kg.m^{-3}		*Z*
				Exp.	$u_c(\rho)$						*Exp.*	$u_c(\rho)$	
1	SC	322.47	40.947	956.3	0.3	0.72	44	SC	322.50	19.491	818.5	0.5	0.40
2	SC	322.48	40.902	956.7	0.3	0.72	45	SC	322.49	19.008	812.8	0.5	0.39
3	SC	322.48	40.153	953.9	0.3	0.71	46	SC	322.50	18.503	806.6	0.6	0.39
4	SC	322.48	39.641	951.7	0.3	0.70	47	SC	322.49	18.008	800.3	0.6	0.38
5	SC	322.47	39.200	950.0	0.3	0.69	48	SC	322.50	17.499	793.5	0.6	0.37
6	SC	322.47	38.434	946.6	0.3	0.68	49	SC	322.51	17.005	786.2	0.6	0.36
7	SC	322.47	38.091	945.0	0.3	0.68	50	SC	322.51	16.502	779.1	0.7	0.36
8	SC	322.46	37.561	942.4	0.3	0.67	51	SC	322.52	16.003	770.9	0.7	0.35
9	SC	322.46	37.005	940.1	0.3	0.66	52	SC	322.52	15.501	761.8	0.7	0.34
10	SC	322.46	36.509	937.7	0.3	0.65	53	SC	322.52	15.012	753.2	0.8	0.33
11	SC	322.46	36.061	935.4	0.3	0.65	54	SC	322.52	14.504	742.9	0.8	0.33
12	SC	322.46	35.500	933.0	0.3	0.64	55	SC	322.52	14.000	731.9	0.9	0.32
13	SC	322.46	34.988	930.2	0.3	0.63	56	SC	322.53	13.501	720.4	1.0	0.31
14	SC	322.47	34.511	928.0	0.3	0.62	57	SC	322.54	13.000	706.7	1.1	0.31
15	SC	322.47	34.062	925.5	0.3	0.62	58	SC	322.53	12.505	691.1	1.2	0.30
16	SC	322.47	33.539	923.2	0.3	0.61	59	SC	322.51	12.003	672.3	1.4	0.30
17	SC	322.47	33.070	920.6	0.3	0.60	60	SC	322.51	11.504	649.9	1.7	0.30
18	SC	322.47	32.536	917.5	0.3	0.60	61	SC	322.49	11.003	621.1	2.1	0.30
19	SC	322.48	32.039	914.6	0.3	0.59	62	SC	322.47	10.501	585.0	2.7	0.30
20	SC	322.47	31.517	912.0	0.3	0.58	63	SC	322.46	9.992	538.0	2.0	0.31
21	SC	322.47	31.027	908.9	0.3	0.57	64	SC	322.45	9.501	460.8	2.5	0.35
22	SC	322.46	30.511	905.8	0.3	0.57	65	SC	322.41	9.006	371.0	1.9	0.41
23	SC	322.47	29.929	902.4	0.3	0.56	66	SC	322.41	8.521	307.2	1.1	0.47
24	SC	322.49	29.507	899.6	0.3	0.55	67	SC	322.41	8.037	254.6	0.7	0.53
25	SC	322.49	29.025	896.4	0.3	0.54	68	SC	322.39	7.504	218.4	0.5	0.58
26	SC	322.48	28.501	892.7	0.4	0.54	69	SC	322.39	7.009	189.5	0.4	0.62
27	SC	322.49	28.018	889.5	0.4	0.53	70	SC	322.41	6.514	166.3	0.3	0.66
28	SC	322.49	27.508	886.3	0.4	0.52	71	Gas	322.39	6.019	145.7	0.2	0.69
29	SC	322.48	27.026	882.9	0.4	0.51	72	Gas	322.39	5.528	127.9	0.2	0.73
30	SC	322.49	26.517	878.8	0.4	0.51	73	Gas	322.39	5.017	111.5	0.2	0.76
31	SC	322.49	26.001	875.4	0.4	0.50	74	Gas	322.39	4.519	96.9	0.2	0.78
32	SC	322.48	25.500	871.4	0.4	0.49	75	Gas	322.39	4.009	82.8	0.2	0.81
33	SC	322.50	25.003	867.7	0.4	0.48	76	Gas	322.39	3.512	70.9	0.1	0.83
34	SC	322.50	24.497	864.4	0.4	0.48	77	Gas	322.40	3.008	58.8	0.1	0.86
35	SC	322.49	24.003	860.4	0.4	0.47	78	Gas	322.40	2.511	48.1	0.1	0.88
36	SC	322.49	23.500	856.5	0.4	0.46	79	Gas	322.39	2.008	37.0	0.1	0.91
37	SC	322.48	23.049	853.3	0.4	0.45	80	Gas	322.39	1.707	31.7	0.1	0.90
38	SC	322.49	22.496	848.2	0.4	0.45	81	Gas	322.40	1.509	27.5	0.1	0.92
39	SC	322.49	22.009	843.9	0.4	0.44	82	Gas	322.39	1.252	22.2	0.1	0.95
40	SC	322.49	21.533	839.7	0.5	0.43	83	Gas	322.40	1.002	17.9	0.1	0.94
41	SC	322.49	21.007	834.7	0.5	0.42	84	Gas	322.40	0.749	13.6	0.1	0.92
42	SC	322.48	20.496	829.2	0.5	0.41	85	Gas	322.39	0.392	7.0	0.1	0.94
43	SC	322.49	20.012	824.3	0.5	0.41							

[a] Standard uncertainties, *u*, are *u(T)* = 0.02 K, *u(p)* = 0.002 MPa for pressures up to 10 MPa and *u(p)* = 0.005 MPa for pressures from 10-40 MPa, for SO_2 *u(z)* = 0.0001 and for CO_2 *u(z)* = 0.0018

Table 7 - Experimental results of the 0.9503 mole CO_2 + 0.0497 mole SO_2 system at 353 K [a]

No	Phase	*T*/K	*p*/MPa	*ρ*/kg.m^{-3}		*Z*	No	Phase	*T*/K	*p*/MPa	*ρ*/kg.m^{-3}		*Z*
				Exp.	$u_c(\rho)$						*Exp.*	$u_c(\rho)$	
1	SC	352.98	39.330	850.5	0.3	0.71	45	SC	352.97	18.007	583.3	1.0	0.47
2	SC	352.98	39.300	850.2	0.3	0.71	46	SC	352.95	17.520	569.4	1.0	0.47
3	SC	352.97	39.009	848.1	0.3	0.71	47	SC	352.96	17.006	552.6	1.1	0.47
4	SC	352.97	38.520	845.7	0.3	0.70	48	SC	352.95	16.515	535.1	1.2	0.47
5	SC	352.98	38.023	842.1	0.3	0.69	49	SC	352.96	16.004	514.7	1.2	0.48
6	SC	352.97	37.499	838.7	0.3	0.69	50	SC	352.95	15.497	493.2	1.3	0.48
7	SC	352.96	36.996	835.2	0.3	0.68	51	SC	352.96	15.003	470.1	1.4	0.49
8	SC	352.97	36.496	831.8	0.3	0.67	52	SC	352.95	14.502	447.3	1.4	0.50
9	SC	352.98	36.013	828.1	0.3	0.67	53	SC	352.96	14.004	422.3	1.4	0.51
10	SC	352.97	35.510	824.7	0.3	0.66	54	SC	352.96	13.501	397.6	1.4	0.52
11	SC	352.97	35.014	821.4	0.4	0.65	55	SC	352.96	12.998	371.8	1.4	0.54
12	SC	352.98	34.563	818.1	0.4	0.65	56	SC	352.95	12.505	346.8	1.4	0.55
13	SC	352.97	34.055	814.5	0.4	0.64	57	SC	352.95	12.000	321.9	1.3	0.57
14	SC	352.96	33.519	809.8	0.4	0.63	58	SC	352.97	11.505	298.8	1.2	0.59
15	SC	352.96	33.014	805.8	0.4	0.63	59	SC	352.96	11.001	276.4	1.1	0.61
16	SC	352.97	32.552	802.4	0.4	0.62	60	SC	352.97	10.506	255.3	1.0	0.63
17	SC	352.96	31.993	797.6	0.4	0.62	61	SC	352.96	10.075	238.1	1.0	0.65
18	SC	352.95	31.494	793.2	0.4	0.61	62	SC	352.95	9.230	209.5	0.3	0.68
19	SC	352.96	31.058	789.4	0.4	0.60	63	SC	352.94	9.008	201.9	0.3	0.68
20	SC	352.97	30.512	784.7	0.4	0.60	64	SC	352.96	8.507	185.5	0.2	0.70
21	SC	352.96	29.991	779.0	0.4	0.59	65	SC	352.94	8.038	170.3	0.2	0.72
22	SC	352.96	29.492	773.9	0.4	0.58	66	SC	352.94	7.498	154.1	0.2	0.75
23	SC	352.97	29.001	768.7	0.4	0.58	67	Gas	352.94	7.017	140.9	0.2	0.76
24	SC	352.96	28.507	764.2	0.5	0.57	68	Gas	352.94	6.516	127.7	0.2	0.78
25	SC	352.96	28.006	758.3	0.5	0.57	69	Gas	352.93	6.001	114.8	0.2	0.80
26	SC	352.96	27.501	752.6	0.5	0.56	70	Gas	352.95	5.490	102.6	0.2	0.82
27	SC	352.98	27.043	747.4	0.5	0.55	71	Gas	352.95	4.997	91.5	0.1	0.84
28	SC	352.97	26.597	742.8	0.5	0.55	72	Gas	352.94	4.493	80.5	0.1	0.86
29	SC	352.96	26.036	736.4	0.5	0.54	73	Gas	352.94	4.003	70.6	0.1	0.87
30	SC	352.96	25.555	731.2	0.5	0.54	74	Gas	352.96	3.495	60.3	0.1	0.89
31	SC	352.95	25.002	723.7	0.5	0.53	75	Gas	352.95	3.009	51.0	0.1	0.90
32	SC	352.95	24.538	717.4	0.6	0.52	76	Gas	352.95	2.800	47.2	0.1	0.91
33	SC	352.96	24.023	710.4	0.6	0.52	77	Gas	352.94	2.504	41.8	0.1	0.92
34	SC	352.96	23.524	703.1	0.6	0.51	78	Gas	352.95	2.248	37.0	0.1	0.93
35	SC	352.95	23.011	694.8	0.6	0.51	79	Gas	352.95	2.002	33.0	0.1	0.93
36	SC	352.95	22.493	686.4	0.6	0.50	80	Gas	352.94	1.742	28.6	0.1	0.93
37	SC	352.95	21.993	677.2	0.7	0.50	81	Gas	352.95	1.507	24.3	0.1	0.95
38	SC	352.96	21.521	668.5	0.7	0.49	82	Gas	352.96	1.248	19.9	0.1	0.96
39	SC	352.96	20.999	657.9	0.7	0.49	83	Gas	352.96	0.982	15.1	0.1	1.00
40	SC	352.96	20.490	647.4	0.8	0.49	84	Gas	352.95	0.740	11.4	0.1	1.00
41	SC	352.96	20.014	636.9	0.8	0.48	85	Gas	352.95	0.511	7.6	0.1	1.03
42	SC	352.95	19.511	624.5	0.8	0.48	86	Gas	352.95	0.402	6.0	0.1	1.03
43	SC	352.96	19.011	611.7	0.9	0.48	87	Gas	352.95	0.306	4.6	0.1	1.02
44	SC	352.97	18.500	597.8	0.9	0.47	88	Gas	352.93	0.202	3.0	0.1	1.03

[a] Standard uncertainties, *u*, are *u(T)* = 0.02 K, *u(p)* = 0.002 MPa for pressures up to 10 MPa and *u(p)* = 0.005 MPa for pressures from 10-40 MPa, for SO_2 *u(z)* = 0.0001 and for CO_2 *u(z)* = 0.0018

Table 8 - Uncertainties with 95% level of confidence ($k=2$) for the measured densities of the CO_2-SO_2 system

			Uncertainties $U(\rho)$			
T / K	Phase	Data	Average		Max.	
		No.	kg.m^{-3}	%	kg.m^{-3}	%
273	Gas	9	0.2	0.7	0.3	2.2
	Liquid	77	0.3	0.0	0.5	0.1
	SC	0	0.0	0.0	0.0	1.0
	Total	86	0.3	0.1	0.5	2.2
283	Gas	17	0.2	0.8	0.7	4.1
	Liquid	76	0.3	0.0	0.6	0.1
	SC	0	0.0	1.0	0.0	1.0
	Total	93	0.3	0.2	0.7	4.1
298	Gas	23	0.3	0.7	1.2	4.4
	Liquid	68	0.4	0.0	0.9	0.1
	SC	0	0.0	1.0	0.0	1.0
	Total	91	0.3	0.2	1.2	4.4
323	Gas	15	0.1	0.4	0.2	1.4
	Liquid	0	0.0	1.0	0.0	1.0
	SC	70	0.6	0.1	2.7	0.6
	Total	85	0.5	0.2	2.7	1.4
353	Gas	22	0.1	0.6	0.2	2.9
	Liquid	0	0.0	1.0	0.0	1.0
	SC	66	0.7	0.1	1.4	0.4
	Total	88	0.5	0.2	1.4	2.9
Total	Gas	86	0.2	0.6	1.2	4.4
	Liquid	221	0.3	0.03	0.9	1.0
	SC	136	0.6	0.12	2.7	1.0
	Total	**443**	**0.4**	**0.2**	**2.7**	**4.4**

Table 9 - Summarised AADs for the measured density of the CO_2-SO_2 system

		Gas	Liquid	SC	Overall
No of Exp. Data		86	221	136	443
Average Absolute Deviation (%)	SRK	2.4	8.2	9.6	7.4
	PR	1.8	3.2	2.4	2.6
	VPT	1.8	1.9	2.6	2.1
	SRK-CO_2	1.9	0.6	0.8	1.0
	PR-CO_2	1.7	0.7	1.1	1.0
	VPT-CO_2	2.2	0.7	1.1	1.1
	SRK-Peneloux	1.9	1.6	4.6	2.6
	PR-Peneloux	1.9	1.1	3.8	2.1
	Multi parameter EoS	1.6	0.2	0.6	0.6
Maximum Absolute Deviation (%)	SRK	13.1	14.6	15.2	15.2
	PR	7.3	7.6	7.3	7.6
	VPT	7.3	8.0	7.5	8.0
	SRK-CO_2	7.4	8.0	6.3	8.0
	PR-CO_2	7.4	7.1	5.8	7.4
	VPT-CO_2	7.4	7.2	5.6	7.4
	SRK-Peneloux	8.5	9.3	11.9	11.9
	PR-Peneloux	7.3	8.0	9.2	9.2
	Multi parameter EoS	7.4	8.0	8.0	8.0

Table 10 - Specific heat capacity calculations for the CO_2 – SO_2 system [a]

T/K	p/MPa	ρ/ kg.m^{-3}	v/ (m^3.mol^{-1})	C_p^0/ (J.K^{-1}.mol^{-1})	C_{pExp}/ (J.K^{-1}.mol^{-1})	$U(C_p)$/ (J.K^{-1}.mol^{-1})	C_{pMP}/ (J.K^{-1}.mol^{-1})	$Dev.$/(%)
				40 MPa				
273.55	40.023	1106.61	4.0671E-05	36.08	76.66	0.14	77.75	1.4
283.33	40.145	1078.76	4.1721E-05	36.34	76.54	0.15	77.88	1.8
298.11	40.060	1031.14	4.3648E-05	37.08	76.92	0.16	78.25	1.7
322.48	40.153	953.87	4.7184E-05	38.25	77.63	0.17	79.25	2.1
352.98	39.330	850.47	5.292E-05	39.58	78.39	0.18	80.78	3.1
				35 MPa				
273.54	35.043	1093.91	4.1143E-05	35.83	80.66	0.17	78.90	-2.2
283.32	34.989	1064.30	4.2288E-05	36.34	81.21	0.18	79.29	-2.4
298.10	35.077	1015.50	4.432E-05	37.08	82.07	0.19	79.98	-2.5
322.46	34.988	930.22	4.8383E-05	38.25	83.86	0.20	81.85	-2.4
352.97	35.014	821.42	5.4792E-05	39.58	85.51	0.21	83.87	-1.9
				30 MPa				
273.55	30.026	1079.37	4.1697E-05	35.83	82.95	0.20	80.32	-3.2
283.32	30.008	1047.27	4.2976E-05	36.34	83.82	0.21	81.00	-3.4
298.11	30.013	996.85	4.5149E-05	37.08	85.34	0.22	82.27	-3.6
322.47	29.929	902.37	4.9877E-05	38.25	88.50	0.24	85.43	-3.5
352.96	29.991	778.96	5.7779E-05	39.58	91.81	0.24	89.08	-3.0
				25 MPa				
273.55	25.039	1063.62	4.3152E-05	35.83	87.42	0.26	82.09	-6.1
283.32	25.025	1029.35	4.4009E-05	36.34	88.89	0.28	83.20	-6.4
298.10	25.050	975.15	4.6687E-05	37.08	91.66	0.29	85.32	-6.9
322.50	25.003	867.65	5.3224E-05	38.26	97.26	0.31	90.70	-6.7
352.95	25.002	723.72	6.4973E-05	39.58	103.82	0.30	97.64	-6.0
				20 MPa				
273.56	20.028	1046.04	4.3026E-05	35.83	91.74	0.42	84.42	-8.0
283.32	20.038	1008.74	4.4617E-05	36.34	93.99	0.43	86.19	-8.3
298.11	20.051	948.90	4.7431E-05	37.08	98.42	0.45	89.81	-8.7
322.49	20.012	824.32	5.4599E-05	38.26	109.99	0.46	99.90	-9.2
352.96	20.014	636.90	7.0666E-05	39.58	121.49	0.42	114.42	-5.8
				15 MPa				
273.57	14.951	1025.38	4.3893E-05	35.83	102.28	0.92	87.64	-14.3
283.32	15.011	984.11	4.5734E-05	36.34	106.18	0.94	90.58	-14.7
298.11	15.011	915.17	4.9179E-05	37.08	115.12	0.94	97.28	-15.5
322.52	15.012	753.20	5.9754E-05	38.26	146.76	0.90	121.74	-17.0
352.96	15.003	470.12	9.5734E-05	39.58	143.82	0.98	141.94	-1.3
			AAD (%)			0.37		5.8

[a] Standard uncertainties, u, are $u(T)$ = 0.02 K and $u(p)$ = 0.005 MPa for pressures from 10-40 MPa

Table 11 - Estimated bubble points from the measured densities for the CO_2 - SO_2 system [a]

Type	Experimental				Prediction (PR-CO_2)		Deviations (%)	
	T/K	p/MPa	ρ/ kg.m^{-3}	$u_c(\rho)$/ kg.m^{-3}	p/MPa	ρ/ kg.m^{-3}	p	ρ
Bubble Point	273.56	3.484	964.4	0.5	3.303	976.4	-5.2	1.2
Bubble Point	283.33	4.304	908.4	0.6	4.221	929.2	-1.9	2.3
Absolute Average Deviation (AAD) (%)							3.6	1.8

[a] Standard uncertainties, u, are $u(T)$ = 0.02 K, $u(p)$ = 0.002 MPa for pressures up to 10 MPa

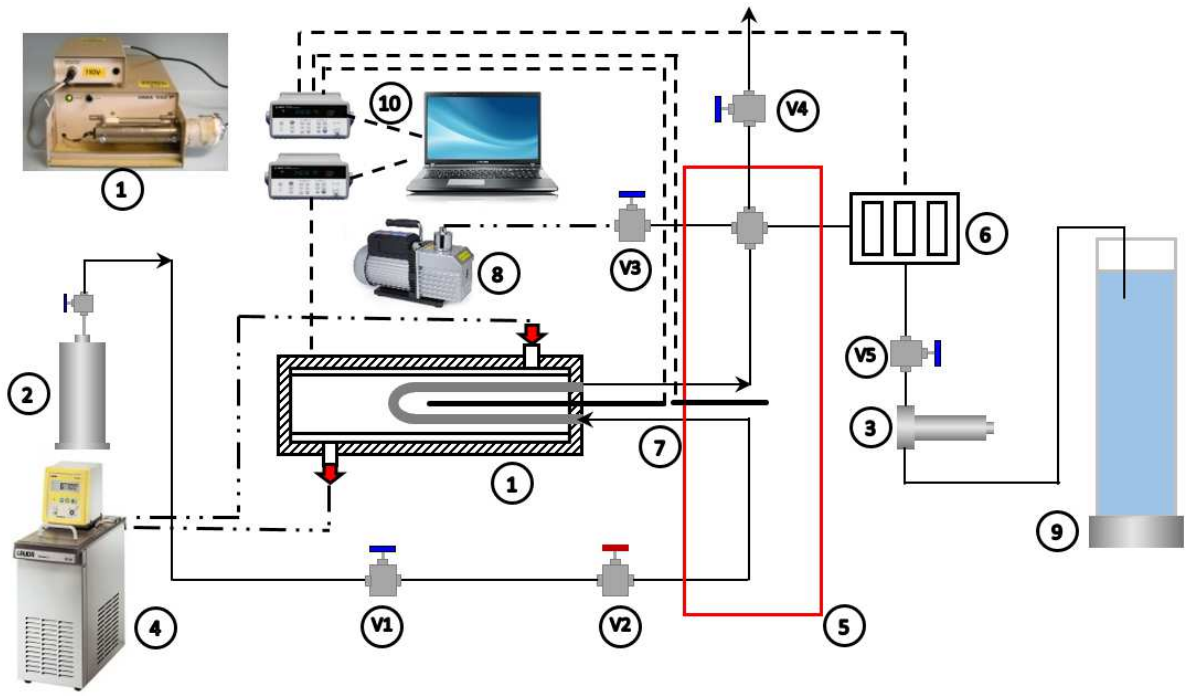

Figure 1 - Schematic diagram of the densitometer apparatus

1) Anton Paar DMA 512 densitometer, 2) High pressure fluid vessel, 3) Capillary Valve , 4) Liquid bath (model: Lauda RE206), 5) Liquid bath of circuit (model: West P6100), 6) Pressure transducers (model: Druck PTX611), 7) Temperature probes, 8) Vacuum pump, 9) Neutralisation column, 10) Data acquisition unit, V1) Circuit valve, V2) Flow controlling ball valve, V3)Vacuum valve, V4) Venting valve, V5) Neutralisation valve

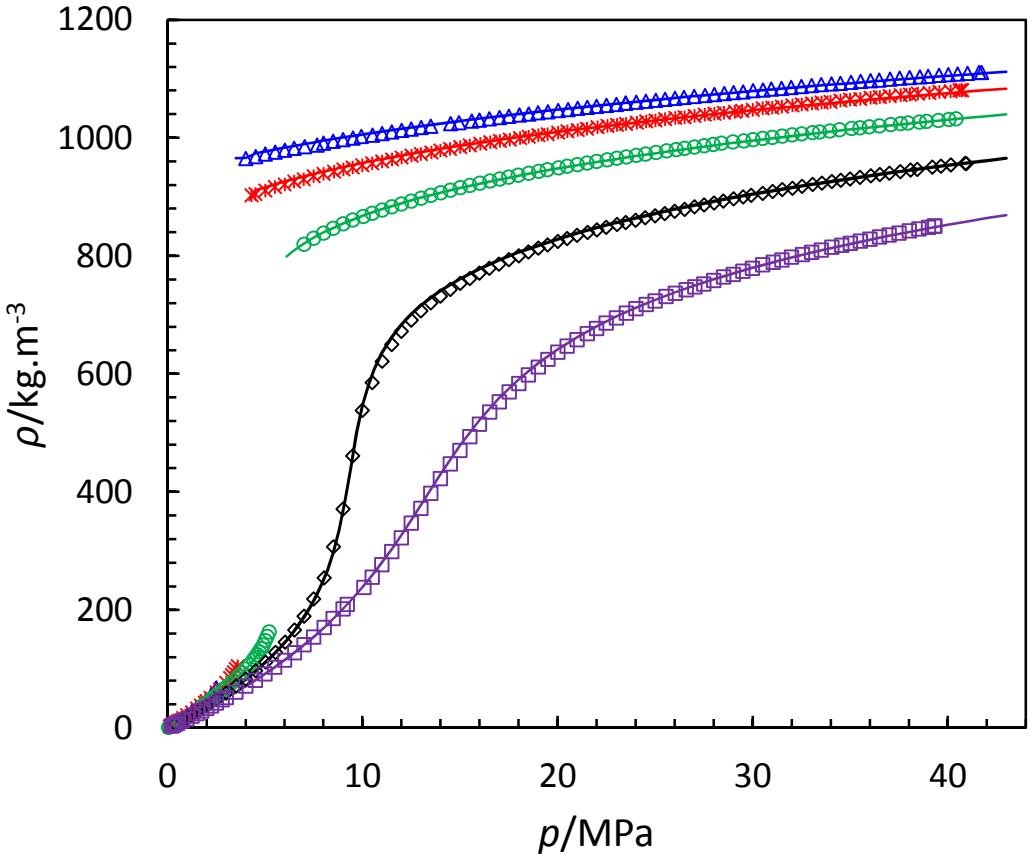

Figure 2 - Experimental and predicted densities of the $CO_2 - SO_2$ system. Experimental results: (Δ) 273. 15 K, (*) 283.15 K, (◊) 323.15 K and (□) 353.15 K for the 0.9503 mole CO_2 + 0.0497 mole SO_2 and (○) 298.15 K for the 0.9478 mole CO_2 + 0.0522 mole SO_2. Lines: Predictions using the multi parameter EoS

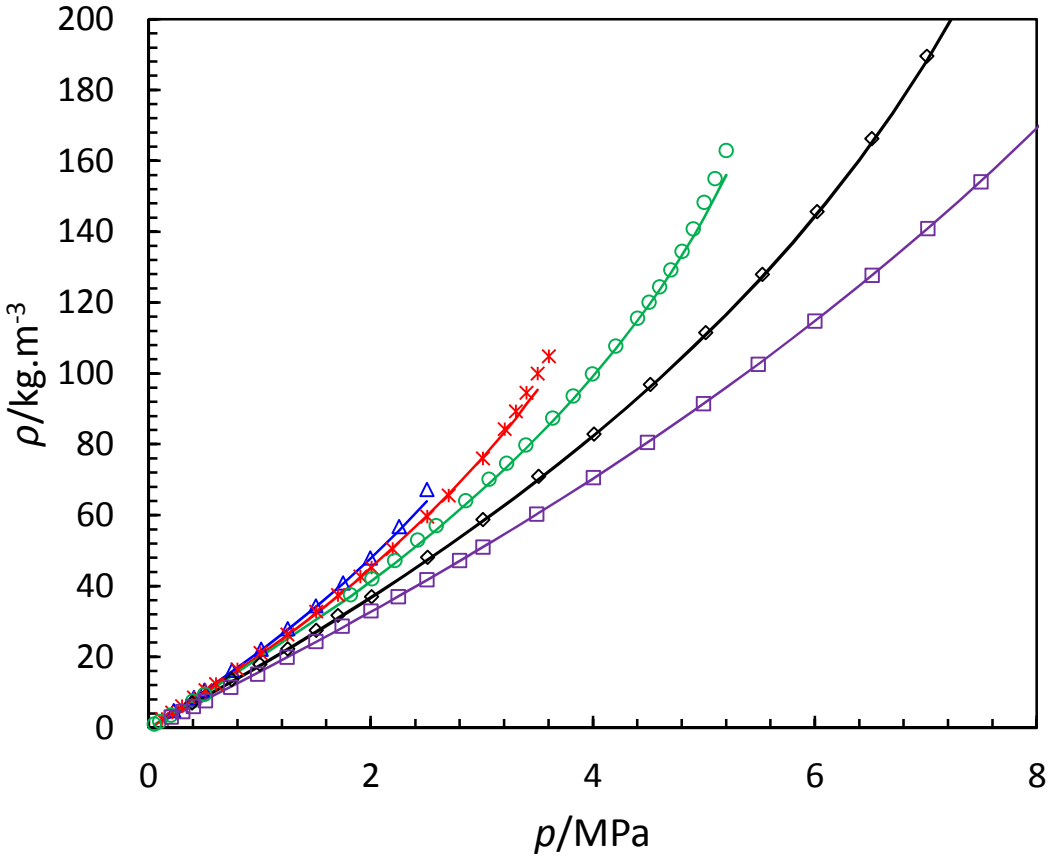

Figure 3 – Low pressure experimental and predicted densities of the CO_2 – SO_2 system. Experimental results: (Δ) 273. 15 K, (*) 283.15 K, (◊) 323.15 K and (□) 353.15 K for the 0.9503 mole CO_2 + 0.0497 mole SO_2 and (○) 298.15 K for the 0.9478 mole CO_2 + 0.0522 mole SO_2. Lines: Predictions using the multi parameter EoS

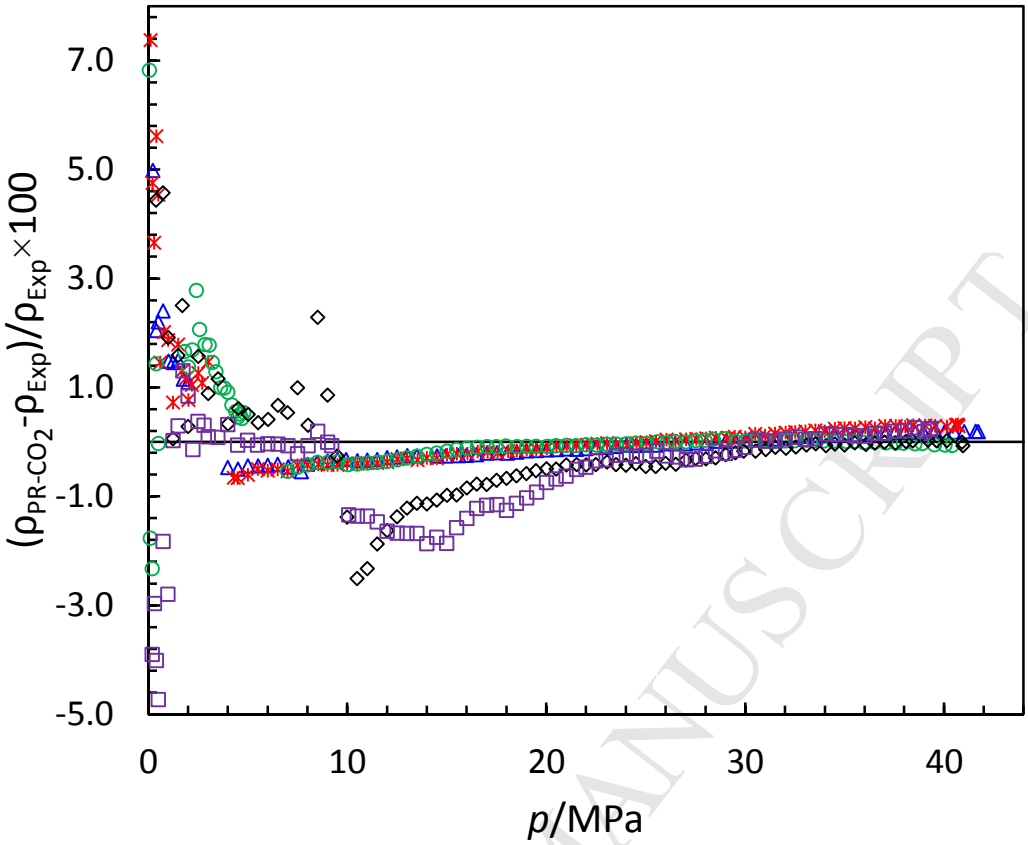

Figure 4 – Deviations of the predictions using the multi parameter EoS from the measured data, (Δ) 273. 15 K, (*) 283.15 K, (◊) 323.15 K and (□) 353.15 K for the 0.9503 mole CO_2 + 0.0497 mole SO_2 and (○) 298.15 K for the 0.9478 mole CO_2 + 0.0522 mole SO_2.

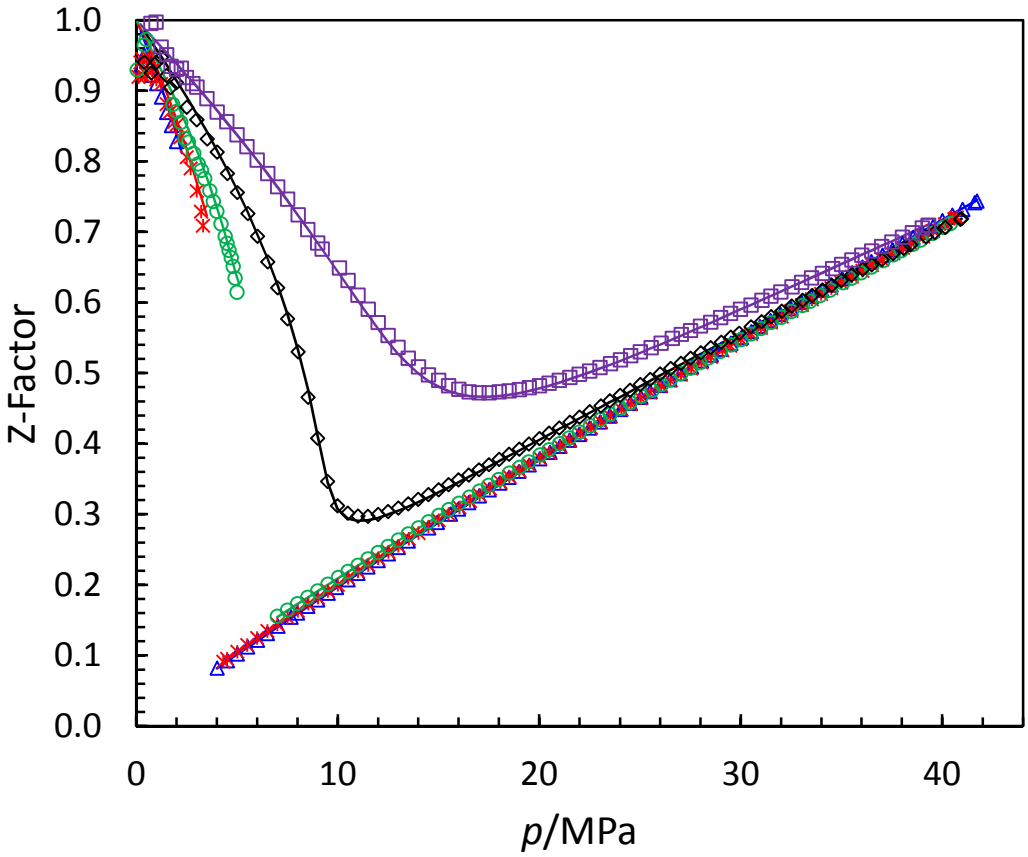

Figure 5 – Compressibility factor of the CO_2 – SO_2 system.
Experimental results: (Δ) 273. 15 K, (*) 283.15 K, (◊) 323.15 K and (□) 353.15 K for the 0.9503 mole CO_2 + 0.0497 mole SO_2 and (○) 298.15 K for the 0.9478 mole CO_2 + 0.0522 mole SO_2. Lines: Predictions using the multi parameter EoS

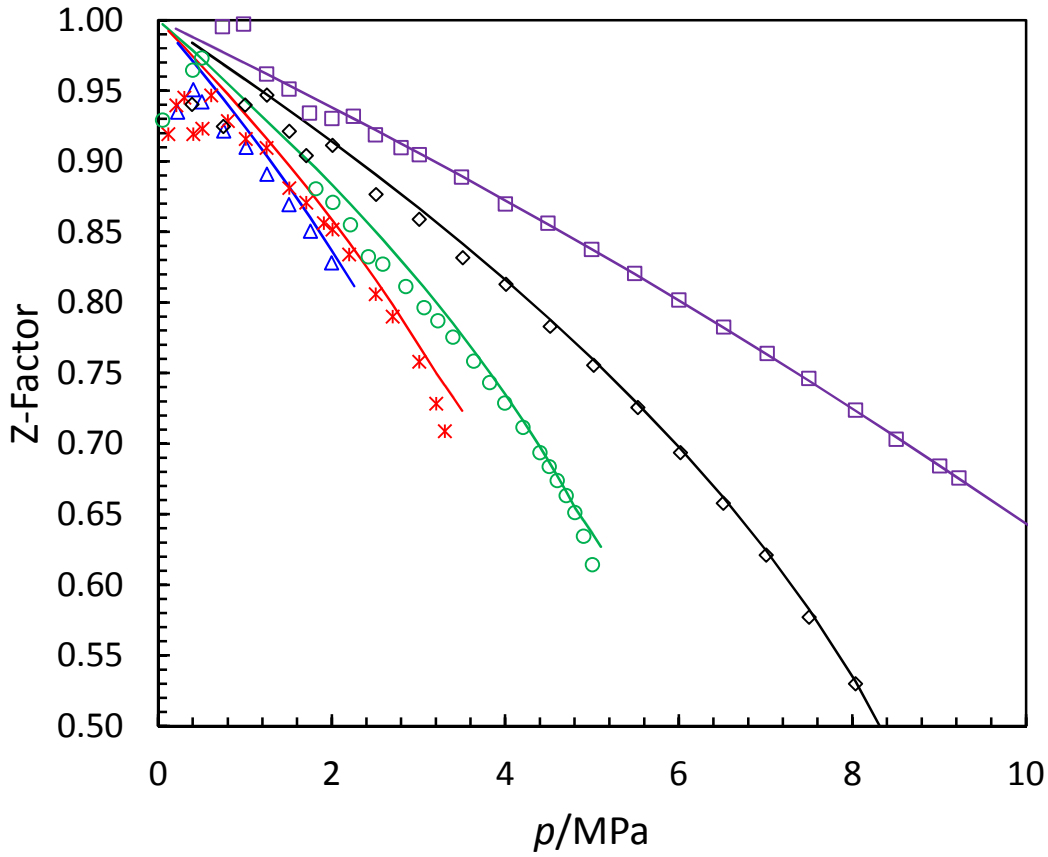

Figure 6 – Compressibility factor of the CO_2 – SO_2 system.
Experimental results: (Δ) 273. 15 K, (*) 283.15 K, (◊) 323.15 K and (□) 353.15 K for the 0.9503 mole CO_2 + 0.0497 mole SO_2 and (○) 298.15 K for the 0.9478 mole CO_2 + 0.0522 mole SO_2. Lines: Predictions using the multi parameter EoS

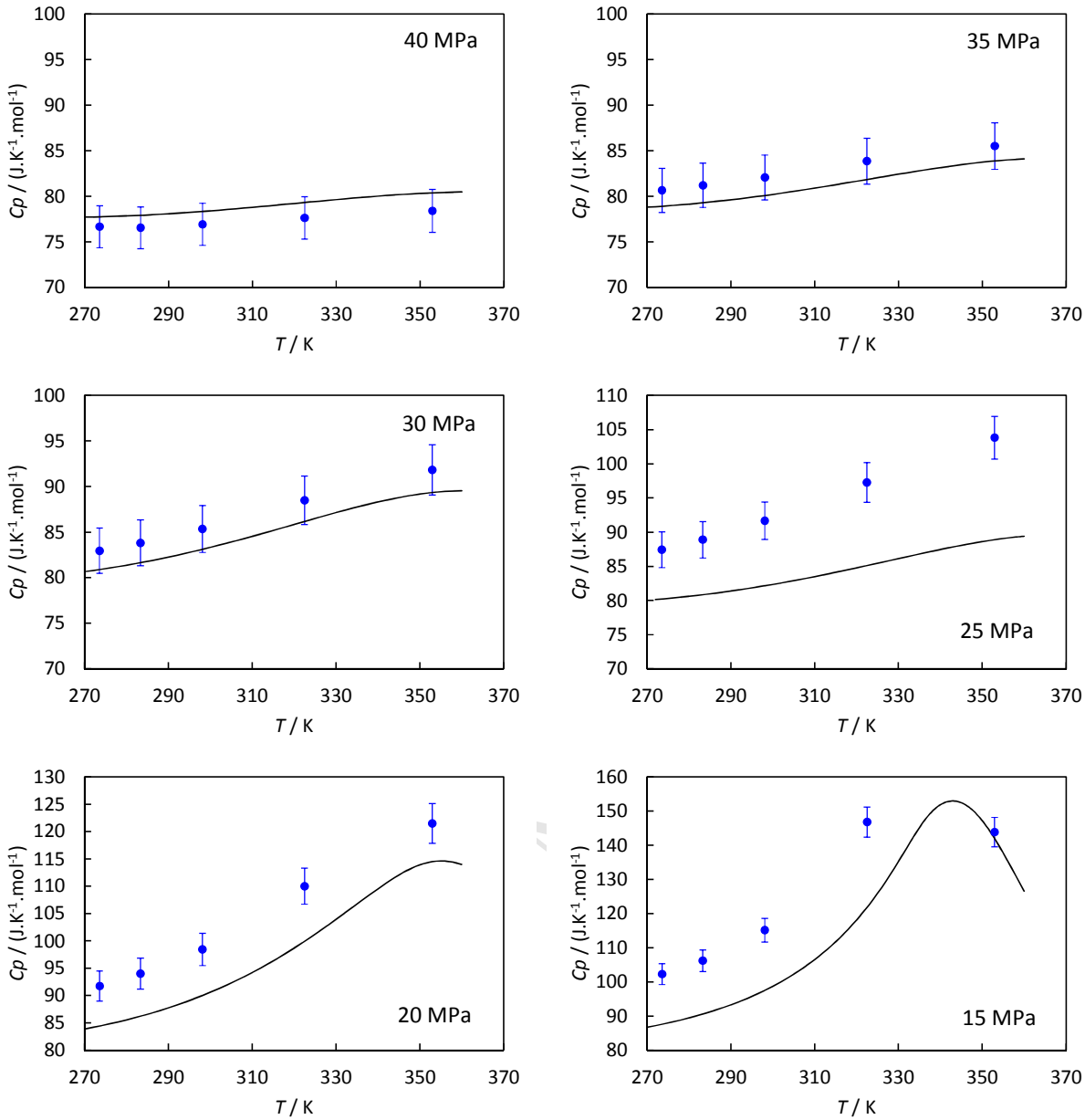

Figure 7 - Specific heat capacity of the CO_2 – SO_2 system (0.9503 mole CO_2 + 0.0497 mole SO_2 at 273. 15 K, 283.15 K, 323.15 K and 353.15 K and 0.9478 mole CO_2 + 0.0522 mole SO_2 at 298.15 K): (●) calculated C_p with 3% error, Lines: predictions using the multi parameter EoS

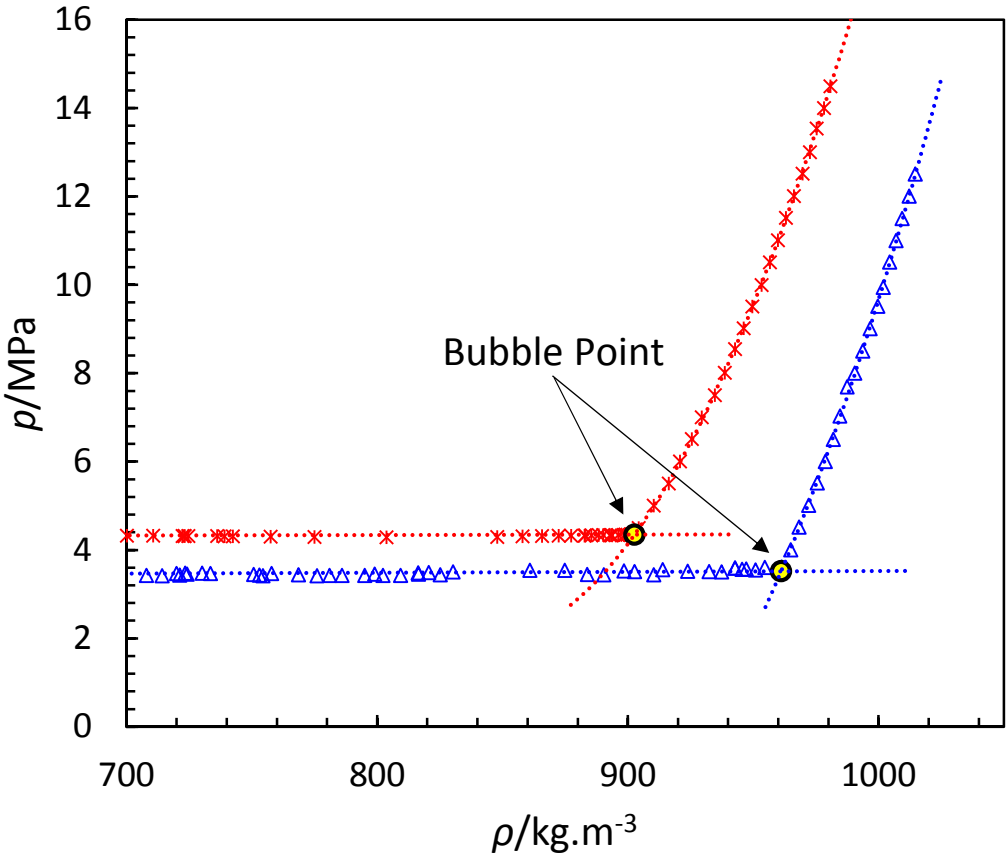

Figure 8 – Bubble point determination of 0.9503 mole CO_2 + 0.0497 mole SO_2 system for different isotherms, (Δ) 273. 15 K, (*) 283.15 K

Appendix A

Equation of State for pure sulphur dioxide [34]**:**

In this work, an industrial short equation from Lemmon & Span was used to predict the thermodynamic properties of pure sulphur dioxide. The equation of state explicit in the Helmholtz energy is expressed in a fundamental form as below:

$$a(\rho,T) = a^0(\rho,T) + a^r(\rho,T) \quad \text{(A-01)}$$

where $a(\rho,T)$ is the Helmholtz energy as function of density and temperature, $a^0(\rho,T)$ is the ideal gas contribution to the Helmholtz energy, and $a^r(\rho,T)$ is the residual Helmholtz energy due to the intermolecular forces. In the dimensionless form, the equation can be expressed as:

$$\frac{a(\rho,T)}{RT} = \alpha(\delta,\tau) = \alpha^0(\delta,\tau) + \alpha^r(\delta,\tau) \quad \text{(A-02)}$$

where $\alpha(\delta,\tau)$ is the dimensionless Helmholtz energy as a function of dimensionless density, $\delta = \rho/\rho_c$, and dimensionless temperature, $\tau = T_c/T$.

The critical density and temperature of sulphur dioxide are 8.195 mol.dm^{-3} and 430.64 K, respectively.

The Helmholtz energy of the ideal gas is given by:

$$a^0 = h^0 - RT - Ts^0 \quad \text{(A-03)}$$

Or, in the dimensionless form is given by:

$$\alpha^0 = a_1 + a_2\tau + \ln\delta + (c_0 - 1)\ln\tau - \frac{c_1\left(\frac{T_c}{K}\right)^{c_2}}{c_2(c_2+1)}\tau^{-c_2} + \sum_{k=1}^{5} v_k \ln[1 - exp(-u_k\tau/T_c)] \quad \text{(A-04)}$$

The constants in the above equation is available in the following Table A-01 for pure sulphur dioxide.

The residual Helmholtz energy term can be find from the work of Span and Wagner for polar fluids including sulphur dioxide [55][56][57]:

$$\alpha^r(\delta,\tau) = n_1\delta\tau^{0.25} + n_2\delta\tau^{1.25} + n_3\delta\tau^{1.5} + n_4\delta^3\tau^{0.25} + n_5\delta^7\tau^{0.875} + n_6\delta\tau^{2.375}exp^{-\delta} + n_7\delta^2\tau^{2.0}exp^{-\delta} + n_8\delta^5\tau^{2.125}exp^{-\delta} + n_9\delta\tau^{3.5}exp^{-\delta^2} + n_{10}\delta\tau^{6.5}exp^{-\delta^2} + n_{11}\delta^4\tau^{4.75}exp^{-\delta^2} + n_{12}\delta^2\tau^{12.5}exp^{-\delta^3} \quad \text{(A-05)}$$

The constants n_1 to n_{12} is also available in Table A-01.

Table A-01 – Constant values of the parameters in the Lemmon & Span EoS

Parameter	value	Parameter	value
v_1	1.0620	n_1	0.93061
u_1/K	775.0	n_2	-1.9528
v_2	1.9401	n_3	-0.17467
u_2/K	1851.0	n_4	0.061524
v_3	0	n_5	0.00017711
u_3/K	0	n_6	0.21615
v_4	0	n_7	0.51353
u_4/K	0	n_8	0.010419
c_0	4.0	n_9	-0.25286
c_1	0.72453×10^{-4}	n_{10}	-0.054720
c_2	1.0	n_{11}	-0.059856
a_1	-4.5328346436	n_{12}	-0.016523
a_2	4.4777967379		

Equation of state for the mixtures [32][33][58]**:**

The Eos explicit in the Helmholtz energy in dimensionless form with the independent variables of reduced mixture density, $\delta = \rho/\rho_r(\bar{x})$, inverse reduced mixture temperature, $\tau = T_r(\bar{x})/T$, and molar composition, $\bar{x}$, is expressed as below for the mixtures:

$$\frac{a}{RT} = \alpha(\delta, \tau, \bar{x}) = \alpha^0(\rho, T, \bar{x}) + \alpha^r(\delta, \tau, \bar{x}) \qquad \text{(A-06)}$$

The ideal gas part, α^0, is given by:

$$\alpha^0(\rho, T, \bar{x}) = \sum_{i=1}^{N} x_i \left[\alpha^0_{0,i}(\delta_{0,i}, \tau_{0,i}) + \ln x_i\right] \qquad \text{(A-07)}$$

where N is the number of components in the mixture, x_i is the mole fraction of component i, and $\alpha^0_{0,i}$ is the ideal gas part of the Helmholtz energy of component i in the mixture. The reduced density and inverse reduced temperature for the pure components are given by:

$$\delta_{0,i} = \rho/\rho_{c,i} \qquad and \qquad \tau_{0,i} = T_{c,i}/T \qquad \text{(A-08)}$$

The residual part of the Helmholtz energy in Equation (A-06) is given by:

$$\alpha^r(\delta, \tau, \bar{x}) = \sum_{i=1}^{N} x_i\, \alpha^r_{0,i}(\delta, \tau) + \Delta\alpha^r(\delta, \tau, \bar{x}) \qquad \text{(A-09)}$$

where $\alpha^r_{0,i}$ is the residual part of the reduced Helmholtz energy of component i and $\Delta\alpha^r$ is the departure function given by:

$$\Delta\alpha^r(\delta, \tau, \bar{x}) = \sum_{i=1}^{N-1} \sum_{j=i+1}^{N} x_i\, x_j F_{ij} \alpha^r_{ij}(\delta, \tau) \qquad \text{(A-10)}$$

where α_{ij}^{r} is the binary specific departure function and F_{ij} is the weighing factor [59]. In this work, F_{ij} is considered equal to zero.

The reducing functions $\rho_r(\bar{x})$ and $T_r(\bar{x})$ are also given by:

$$\frac{1}{\rho_r(\bar{x})} = \sum_{i=1}^{N} x_i^2 \frac{1}{\rho_{c,i}} + \sum_{i=1}^{N-1} \sum_{j=i+1}^{N} 2x_i\, x_j \beta_{v,ij}\gamma_{v,ij} \frac{x_i + x_j}{\beta_{v,ij}^2 x_i + x_j} \frac{1}{8}\left(\frac{1}{\rho_{c,i}^{1/3}} + \frac{1}{\rho_{c,j}^{1/3}}\right)^3 \qquad \text{(A-11)}$$

and

$$T_r(\bar{x}) = \sum_{i=1}^{N} x_i^2\, T_{c,i} + \sum_{i=1}^{N-1} \sum_{j=i+1}^{N} 2x_i\, x_j \beta_{T,ij}\gamma_{T,ij} \frac{x_i + x_j}{\beta_{T,ij}^2 x_i + x_j} \left(T_{c,i} T_{c,j}\right)^{0.5} \qquad \text{(A-12)}$$

The binary parameters which allow for the arbitrary symmetric and asymmetric shapes of the functions were set as below:

$$\beta_{v,ij} = 1.0 \quad and \quad \gamma_{v,ij} = 1.0 \qquad \text{(A-13)}$$

$$\beta_{T,ij} = 0.99686 \quad and \quad \gamma_{T,ij} = 1.0093 \qquad \text{(A-14)}$$

These parameters were adjusted on the available VLE data.

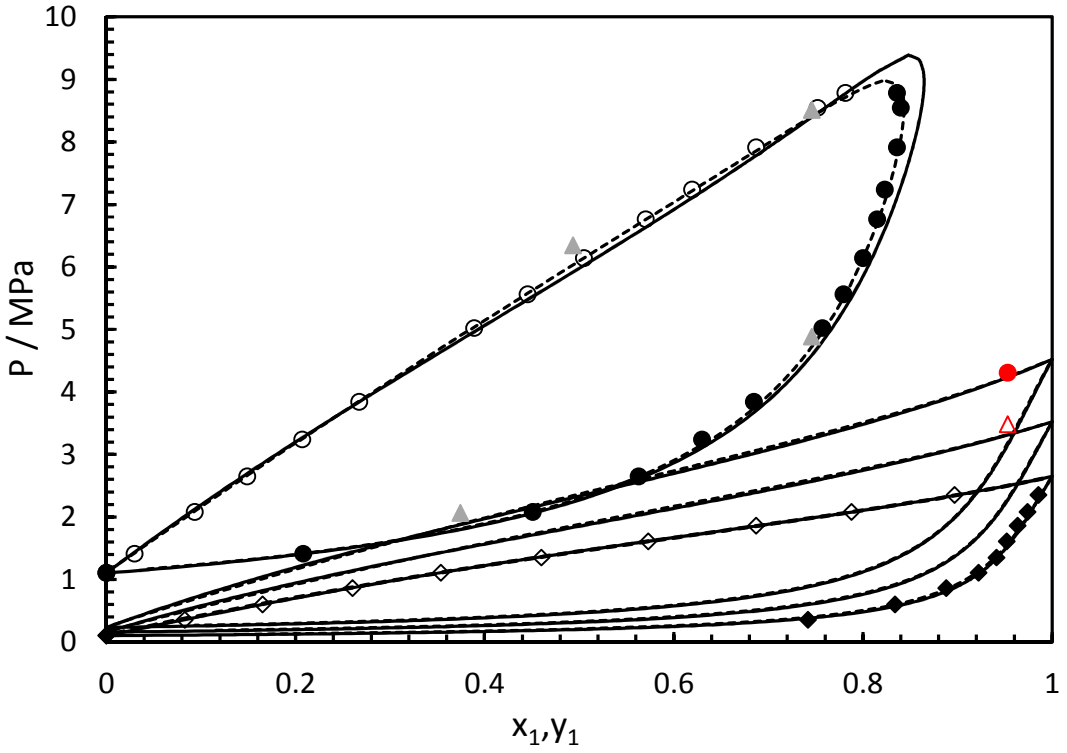

Figure A.1 Pressure – composition diagram of the CO_2 (1) + SO_2 (2) system. From Coquelet et al. [25]: (○), Liquid phase T = 333.15 K; (●), Vapour phase T = 333.15 K; (◇), Liquid phase T = 263.15 K. (◆), Vapour phase T=263.15 K; From Caubet [23] (▲), Liquid Phase T = 333 K; From this work : (●), Bubble point measured at T = 283.33 K, (△), Bubble point

measured at T = 273.56 K . Black lines: calculated VLE lines using the multi parameter EoS. Dashed lines: calculated VLE lines using the PR-EoS model with k_{ij}=0.02.